



Holocene lake response to glacier and catchment changes on the eastern Tibetan Plateau from quantitative conductivity reconstructions based on sedaDNA-derived macrophyte records

Wenjia Li^{a,b,c}, Xianyong Cao^{b,**}, Kathleen Stoof-Leichsenring^a, Xiaohuan Hou^b, Shi-Yong Yu^d, Fang Tian^e, Ulrike Herzschuh^{a,f,g,*}

^a Polar Terrestrial Environmental Systems, Alfred Wegener Institute Helmholtz Centre for Polar and Marine Research, Potsdam, 14473, Germany

^b Group of Alpine Paleocology and Human Adaptation (ALPHA), State Key Laboratory of Tibetan Plateau Earth System, Environment and Resources (TPESER), Institute of Tibetan Plateau Research, Chinese Academy of Sciences, Beijing, 100101, China

^c University of Chinese Academy of Science, Beijing, 100049, China

^d School of Geography, Geomatics, and Planning, Jiangsu Normal University, Xuzhou, 221116, China

^e College of Resource Environment and Tourism, Capital Normal University, Beijing, 100048, China

^f Institute of Environmental Science and Geography, University of Potsdam, Potsdam, 14476, Germany

^g Institute of Biochemistry and Biology, University of Potsdam, Potsdam, 14476, Germany

ARTICLE INFO

Handling Editor: P Rioual

Keywords:

SedaDNA
Palynological analysis
Grain-size end-member modelling
Tibetan plateau
Lake conductivity

ABSTRACT

Understanding the response of long-term aquatic environmental changes in lakes to ongoing climate change and human activities is key to forecasting future lake conditions. In this study, we infer the Holocene limnological changes in Emu Co, a proglacial lake in Nianbaoyuze on the eastern Tibetan Plateau, from sedimentary ancient DNA (sedaDNA) data, and palynomorph, element, lithological, and grain-size analyses. We developed a transfer function based on Siberia and Tibet/China surface sedimentary DNA and applied it to Emu Co sedaDNA to trace lake conductivity changes. The results show that the conductivity of Emu Co was high during 12.6–9.7 cal ka BP, often surpassing 1000 $\mu\text{S cm}^{-1}$, driven by elevated summer solar radiation. The freshwater influx from glacial meltwater and precipitation, however, reduced the lake's conductivity as the climate warmed and humidified. This led to a decrease in the abundance of taxa characterised by high conductivity. Freshwater pulses, triggered by climatic fluctuations, likely led to significant variations in conductivity within the overarching downward trend. By 8 cal. ka BP, lake recharge conditions stabilised and conductivity reached a lower level of $\sim 70 \mu\text{S cm}^{-1}$. The warm and humid mid-Holocene (8–5 cal. ka BP) provided suitable habitat conditions for many submerged freshwater taxa. After 5 cal. ka BP, the growth of submerged taxa was restricted, as indicated by a shift from asexual to sexual reproduction in macrophytes, likely in response to suboptimal conditions of a colder and drier climate. Since 1 cal. ka BP, human activities might have increased lake nutrient levels, with an enhanced richness of macrophytes. Our results indicate how millennial-scale hydrological changes in a lake are related to glacial retreat and catchment changes in the alpine region of the Tibetan Plateau, which is today facing climate change much greater than the global average.

1. Introduction

Lakes on the Tibetan Plateau (TP) have experienced pronounced shifts in hydrology in recent decades, such as rising water levels,

decreasing salinity and increasing nutrient levels (Zhang et al., 2020; Shang et al., 2023). Climate change alongside human activities are acknowledged as significant drivers of these aquatic environmental changes (Ma et al., 2010; Woolway et al., 2020). Temperature increases,

* Corresponding author. Polar Terrestrial Environmental Systems, Alfred Wegener Institute Helmholtz Centre for Polar and Marine Research, Potsdam, 14473, Germany.

** Corresponding author. Group of Alpine Paleocology and Human Adaptation (ALPHA), State Key Laboratory of Tibetan Plateau Earth System, Environment and Resources (TPESER), Institute of Tibetan Plateau Research, Chinese Academy of Sciences, Beijing, 100101, China

E-mail addresses: xcao@itpcas.ac.cn (X. Cao), Ulrike.Herzschuh@awi.de (U. Herzschuh).

<https://doi.org/10.1016/j.quascirev.2024.108806>

Received 2 April 2024; Received in revised form 26 June 2024; Accepted 27 June 2024

Available online 20 July 2024

0277-3791/© 2024 The Authors. Published by Elsevier Ltd. This is an open access article under the CC BY license (<http://creativecommons.org/licenses/by/4.0/>).

coupled with augmented precipitation and accelerated glacier and snow melt, have directly expanded alpine lake volumes (Ye et al., 2008; Zhou et al., 2015; Zhang et al., 2020), elevating water levels and diminishing salinity (Song et al., 2014; Zhou et al., 2022). The associated wetting trend boosts rock weathering, thereby altering surface water chemistry (Gibbs, 1970). Additionally, the pastoral lifestyle characteristic of the TP has increased the nutrient load of the lakes (Han et al., 2023; Shang et al., 2023). Understanding the processes that drive long-term changes in hydrological conditions of the TP lakes, which are part of the "Asian Water Tower", is essential for maintaining local ecosystems and securing water supply in downstream areas (Immerzeel et al., 2010; Yao et al., 2022). However, the short duration of observational records limits our comprehension, emphasising the importance of developing and analysing extended ecological time series.

The lakes on the TP provide sedimentary archives that offer valuable clues for exploring long-term lake water conditions change. Numerous sediment-derived proxies (e.g. grain size, sediment geochemistry, fossil remains, biomarkers) are used for lake palaeohydrology. Modern assemblages of ostracods, chironomids, and diatoms have been used to set up multivariate transfer functions which have been deployed to quantitatively reconstruct conductivity, salinity, and lake-level changes on the TP (Yang et al., 2003; Mischke et al., 2007; Yu et al., 2023). However, taphonomic issues including poor preservation and a limited taxonomic resolution restrict the widespread applicability of these methods.

Aquatic macrophytes are vascular plants growing in or near water that can be classified as floating, submerged, or emergent (Chambers et al., 2008). As primary producers, their growth and energy metabolism are directly impacted by abiotic factors like water temperature, salinity, and the nutrient status of the lake. Thus, the distinct niches of these macrophytes offer insights into their ecological drivers. A range of macrophyte traits have been identified. For instance, a study of submerged macrobenthic communities across 300 Danish lakes identified several species of isoetids and *Potamogeton* as markers of nutrient-poor lake conditions (Søndergaard et al., 2010). *Stuckenia pectinata* is distinguished by its increased productivity in lakes with elevated conductivity (Herzschuh et al., 2010a) and can also thrive in lakes with high bicarbonate concentrations (James, 2008). Hitherto the composition and abundance of aquatic macrophytes has been used as a (semi-)qualitative proxy for past limnological conditions (Birks, 2001). Examples include using the Holocene macrofossil record from Lake Njargajavri in Finnish Lapland for lake-level reconstructions (Väliranta et al., 2005), analysing stable carbon isotope compositions of macrophyte remains from Lake Luanhaizi on the northeastern TP to assess nutrient dynamics since 45 cal. ka BP (Herzschuh et al., 2010b), and employing palynological records from Changdang Lake in China to trace changes in aquatic plant communities over the past century due to hydrological and nutrient influences (Ge et al., 2018). However, the limitations of these traditional analysis methods have been recognised. For instance, the remains of macrofossils are usually relatively scarce, making their study requires large quantities of sediment (Birks and Birks, 2000). Interpretation of palynological records is challenged by low taxonomic resolution and the commonly found asexual reproduction strategies of aquatic macrophytes (Sayer et al., 1999).

The recently developed sedimentary ancient DNA (sedaDNA) analysis is a method that combines large data volumes, high taxonomic resolution, and standardised identification (Birks and Birks, 2016; Capo et al., 2021). Aquatic macrophytes have a higher likelihood of their DNA being preserved in lake sediments, as opposed to terrestrial plants, making them ideal for sedaDNA analysis (Alsos et al., 2022; Stooß-Leichsenring et al., 2022). The aquatic vegetation types recorded in the surface sediments are comparable or even superior to the in-lake vegetation surveys when comparing the surface sediment DNA (sedDNA) with the in-lake vegetation survey data (Alsos et al., 2018). Recent studies employing sedaDNA for reconstructing aquatic macrophyte compositions have provided invaluable insights into their historical

biological structure and function change (Baisheva et al., 2023; Karachurina et al., 2023). However, despite the TP having the largest group of alpine lakes in the world (Wang and Dou, 1998), the application of sedaDNA technology has been limited to terrestrial plant reconstruction and diversity studies (Li et al., 2021; Liu et al., 2021a, 2021b), neglecting its potential in aquatic macrophyte research. Nevertheless, Stooß-Leichsenring et al. (2022) have compiled a set of sedaDNA data from lakes across the TP and Siberia, presenting a promising foundation for quantitative reconstructions in this field.

To examine the changes in lake water conditions and responses of macrophytes to abiotic factors (e.g. climate changes and glacier melt) and anthropogenic forcing, we selected Emu Co, a glacier and precipitation-fed lake located in the eastern TP as our study site. We conducted sedaDNA metabarcoding along with palynological analysis to reconstruct the variation in aquatic macrophyte composition in Emu Co over the past 12.6 cal ka BP. A transfer function based on sedaDNA was developed to track Holocene conductivity change trajectories. In addition, we explored the impacts of catchment-related changes on the aquatic environments of the lake and the composition of the aquatic macrophytes, with the help of physical and chemical indicators, such as elements, grain size, and organic carbon.

2. Materials and methods

2.1. Study site

Emu Co (33.232°–33.233°N, 100.989°–101.001°E; 4020 m a.s.l.; Fig. 1) is located on the eastern margin of the TP, within the eastern section of the Bayan Har Mountains, west of Nianbaoyuzhe Mountain. It is a lake that remains from glacial retreats (Fig. 1c; Lehmkühl and Liu, 1994). Nowadays, a glacier is still present on the highest peak of Nianbaoyuzhe (5369 m a.s.l.) in the upper reaches of the Emu Co catchment. The study area exhibits typical plateau continental climate characteristics, with distinct cold and warm seasons over the year. The data from the nearest meteorological station to Emu Co, Jiuzhi County, for the period 1981–2010 CE, records a mean annual precipitation of 732.5 mm, with precipitation primarily concentrated in the summer months (June to August). The mean annual temperature is 1.1 °C, with the highest mean temperature occurring in July or August (Fig. 1d; National Meteorological Information Center, 2019).

2.2. Sediment core and chronology

In May 2021, a 387.5-cm sediment core (33°13'52" N, 100°59'20" E; 4020 m a.s.l.) was obtained from a water depth of 11.4 m using a gravity corer (VC-D, SDI, Dallas, TX, USA) with a 60 mm diameter. The core was split into two halves and stored at 4 °C at the State Key Laboratory of Tibetan Plateau Earth System, Environment and Resources prior to analysis. Half of the core was subsampled at 1-cm intervals in a previously cleaned room using sterile tools, a full bodysuit, facemask, and gloves following the protocol described by Parducci et al. (2017) and von Hippel et al. (2022). The age-depth model for the core was established by combining radioisotopes, including ²¹⁰Pb and ¹³⁷Cs, with accelerator mass spectrometry (AMS) radiocarbon dating. We performed ²¹⁰Pb and ¹³⁷Cs radioactivity intensity measurements on the upper 20 cm of the sediment, and ¹⁴C dating was performed on 10 stratigraphical levels of bulk organic matter at different core depths (Fig. 2; Table S1). To account for the lake reservoir effect (Yu et al., 2007; Hou et al., 2012), a difference (2389 years) between the ¹⁴C dates and the results of the ²¹⁰Pb analyses of the top 0–0.5 cm core sample was subtracted from all other ¹⁴C ages. Other detailed information regarding the age-depth model is given in Li et al. (2023). The average sedimentation rate of the core is 0.06 cm yr⁻¹ (Fig. 2).

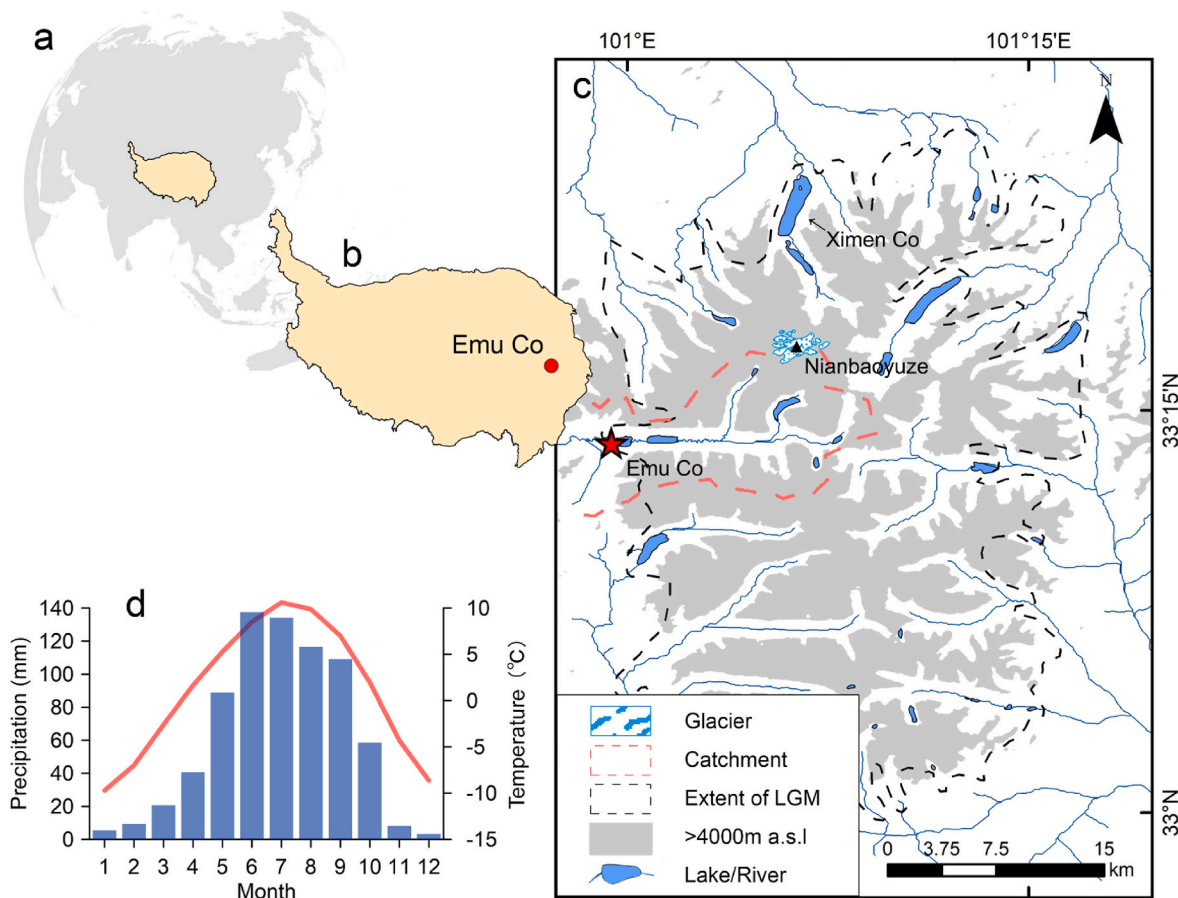


Fig. 1. Settings of the study area. (a) Location of the Tibetan Plateau; (b) Location of Emu Co on the Tibetan Plateau; (c) Nianbaoyuze Mountains (grey shading) in relation to Emu Co and the extent of glaciers nowadays and during the Last Glacial Maximum (LGM; [Lehmkuhl, 1998](#)); (d) Climatology of Jiuzhi County (1981–2010 CE).

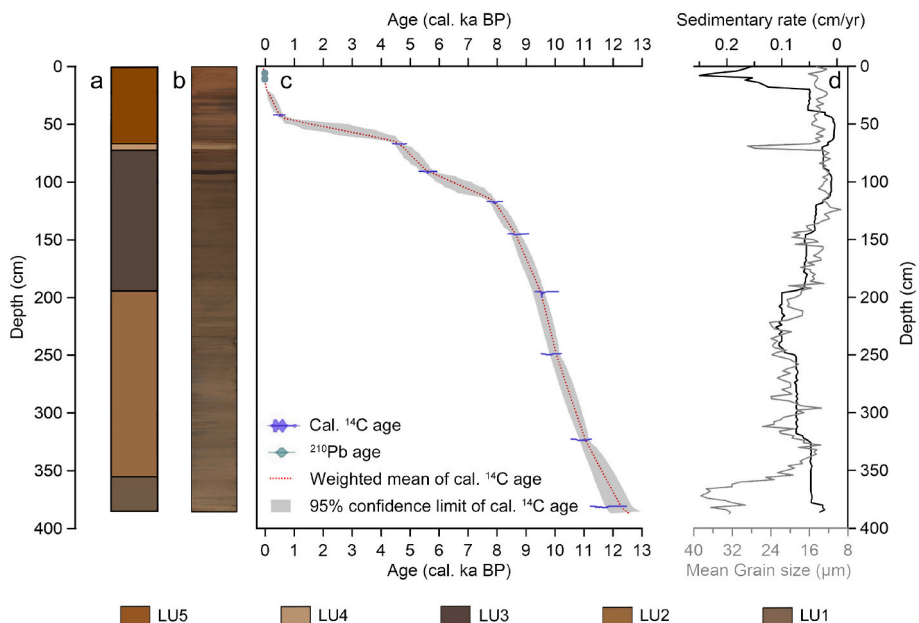


Fig. 2. (a) Lithology of Emu Co lake sediment core with a colour code demarcating the lithological units (LU; LU1: brown, very coarse silt, organic-poor; LU2: brown coarse silt; LU3: brown to dark yellowish brown medium silt, organic-rich; LU4: light brown coarse silt; LU5: dark brown medium silt with intermittent brown layers); (b) Photograph of Emu Co lake sediment core; (c) Age-depth model and (d) sedimentary rate and mean grain size of the Emu Co lake sediment core.

2.3. Geochemical and sedimentological analyses

The split core was imaged and analysed using an ITRAX XRF core scanner equipped with a molybdenum tube providing X-ray energy from the State Key Laboratory of Tibetan Plateau Earth System Science, Institute of Tibetan Plateau Research, CAS. All elements were scanned with a voltage of 30 kV, current of 50 mA, and an exposure time of 10 s. The units are expressed as counts per second (cps) and the counting was conducted at 0.5 mm. The elements were divided by the coherent radiation (coh) count as this is useful for normalising for primary intensity from the tube (Ohlendorf et al., 2015). In addition, to reduce closed-sum effects (Croudace and Rothwell, 2015; Weltje and Tjallingii, 2008), we performed an additive log-ratio (ALR) transformation on the elemental ratios.

Total nitrogen (TN), total carbon (TC), and total organic carbon (TOC) were measured on subsamples at 2-cm intervals. TN and TC were measured using freeze-dried and ground to 147 µm samples of 0.3 g on an EMA3000 elemental analyzer (Thermo Fisher Scientific, USA). TOC was quantified using 0.3 g of HCl-treated samples using the same instrument at Jiangsu Normal University.

About 0.2 g of freeze-dried samples at 2-cm intervals were selected for grain-size analysis. The samples were treated with an excess of 30% H₂O₂ and 10% HCl to remove organic matter and carbonates. The samples were then rinsed with deionized water and after 24 h of standing the supernatant was removed. 10 mL of 0.05 N (NaPO₃)₆ was added to promote dispersion and the samples were shaken on an ultrasonicator for 10 min before analysis. Grain size was measured using a Malvern Mastersizer 3000 laser particle sizer (Malvern, UK) and the final result is the average of three replicate measurements. Sorting factors were calculated using GRADISTAT software (Blott and Pye, 2001) based on Folk and Ward graphical methods (1957). To extract environmental information from the grain-size data and to identify the source or sediment transport process of Emu Co sediments, the end-member modelling algorithm (EMMA) was used to extract genetically meaningful end-members from the full array of grain-size data (Weltje, 1997; Dietze et al., 2012).

2.4. Palynological analysis

A total of 116 samples from the cores were analysed for palynology. Exotic *Lycopodium* spores (10,315 spores per tablet) were first added to each sample to calculate pollen concentration (Stockmarr, 1971). We treated the samples sequentially for carbonate, silicate, and humic acid using 10% HCl-10% NaOH-40% HF, then sieved through a 7 µm mesh and mounted with silicone oil (Faegri et al., 1989). Palynological identification was carried out under an optical microscope at 400× magnification, referring to palynological reference slides produced by Cao et al. (2021) and the palynological atlases edited by Tang et al. (2020) and Wang et al. (1995). A minimum of 500 pollen grains were counted per sample. For this study, only aquatic taxa were considered. Additionally, the alga *Pediastrum* was identified through palynological analysis.

2.5. SedaDNA analysis

The extraction of the sedaDNA from 62 sediment core samples was carried out in the palaeogenetic laboratories at the Alfred Wegener Institute in Potsdam, Germany. DNA extraction was performed under a dedicated UV working hood using the DNeasy PowerSoil DNA Isolation Kit (Qiagen, Germany) with 250 mg of input material. To obtain enough DNA for polymerase chain reaction (PCR) amplification, we performed two extractions of each sample with a total sediment usage of 500 mg. For each batch of 8 samples, an extraction blank was run alongside the samples to control for possible contamination of chemicals in the DNA extraction kit. Then, extracts were combined, concentrated using the GeneJet PCR Purification Kit (Thermo Scientific, USA) and quantified

using the broad range dsDNA Assay Kit with the Qubit 2 Fluorometer (Invitrogen, USA).

PCR-setups were prepared in the palaeogenetic laboratories at AWI using a dedicated UV working hood. We used the plant universal primers g and h that target the short region of the *trnL* intron in the chloroplast genome (Taberlet et al., 2007). The PCR mix contained 12.8 µL of DEPC water (VWR, Germany), 2.5 µL of 10 × HiFi buffer, 2.5 µL of dNTPS (2.5 mM), 1 µL of Bovine Serum Albumin (20 mg mL⁻¹, VWR, Germany), 1 µL of MgSO₄ (50 mM), 0.2 µL of Platinum™ Taq High Fidelity DNA Polymerase and buffer (Invitrogen, USA), 3 µL of extracted sedaDNA (diluted to 3 ng µL⁻¹), and 1 µL each of forward (g) and reverse (h) primer. The forward and reverse primers were modified with a NNN-8 bp tag at the 5' end to ensure demultiplexing of samples after sequencing (Coissac et al., 2012; De Barba et al., 2014). The post-PCR workspace for thermal cycling, purification, and pooling is physically separate from the palaeogenetic laboratories to avoid contamination of ancient DNA with modern or amplified DNA. The PCR was run at 94 °C for 5 min of initial denaturation, followed by 40 cycles of 30 s at 94 °C, 30 s at 50 °C, 30 s at 68 °C, and a final extension at 72 °C for 10 min. Each batch of PCR included a 'No template control' (NTC) containing only the PCR chemical and the extraction blank control corresponding to the analysed sample batch. The PCR reactions were repeated three times using different tag combinations to allow a separation of each PCR replicate during the bioinformatic analysis. PCR replicates of the same sample were pooled and purified using MinElute kits (Qiagen, The Netherlands). The DNA concentration was measured by using a broad-range dsDNA Assay Kit and the Qubit 4 Fluorometer (Invitrogen, USA). Purified samples were pooled into an equimolar mixture which was purified again using the MinElute kit (Qiagen, The Netherlands) to aim for the final DNA concentration of 70 ng µL⁻¹ required for sequencing. Library preparation using the MetaFast library protocol and amplicon sequencing on an Illumina NextSeq device using 2 × 150 bp paired-end was performed by Fasteris SA, Switzerland.

2.6. Bioinformatic analyses and sedaDNA data quality control

Analysis of the Illumina raw sequencing data was done using the OBITools3 software (Boyer et al., 2016) with the following functions including *obi alignpairedend* (merging forward and reverse reads), *obin gsfiler* (assign PCR replicates to read counts) and *obi uniq* (dereplicate the read counts). Then, *obi grep* was used to filter for sequences <1 bp in length and <1 read counts and *obi clean* was applied to remove PCR and sequencing errors. Finally, DNA sequences were taxonomically assigned using an obitools database originating from the EMBL Nucleotide Sequence Database (Release 143, April 2020) using the *ecotag* function. The recovered amplicon sequence variants (ASVs) were filtered for a 100% similarity to references in the database.

We ran in total 21 extraction blanks (EBs) and 34 no-template controls (NTCs) along with the 186 samples. This study focused exclusively on ASVs assigned to aquatic macrophyte taxa. After excluding non-aquatic macrophyte taxa, ASVs reads in EBs and NTCs accounted for 0% and 0.26% of the total reads, respectively (Table S2). The majority of reads in the NTCs originate from NTC22. However, results from the Non-metric multidimensional scaling (NMDS) analysis shows a wide difference between the ASV composition of NTC22 and the associated samples. Furthermore, the reproducibility of the NTC22-related samples is good (Fig. S1). Therefore, we did not remove the ASVs in subsequent analyses. For further denoising, ASVs in the dataset with a taxonomic level higher than family were removed and only those ASVs with frequencies ≥2 were retained for the ensuing data processing. Following the naming convention by Stooft-Leichsenring et al. (2022), we maintained distinct ASVs and assigned them numbers corresponding to their taxonomic identities (details provided in Supplementary file 2).

2.7. Statistical analyses and conductivity reconstruction based on sedaDNA

All analyses in this study were conducted in R (R Core Team, 2021). To mitigate the impact of total sedaDNA read counts on diversity inference across Emu Co core samples, we selected the smallest total read count in our dataset (748 reads) as the standard for resampling and rarefied these data 100 times (detail of the rarefied mean data are given in Supplementary file 2). Percentages of aquatic macrophyte taxa were subsequently calculated based on the resampled data. The stratigraphically constrained cluster analysis (CONISS, Grimm, 1987) was used to divide the biostratigraphic zones. Richness (i.e., the number of ASVs) was computed using the iNext function from the iNext package (Hsieh et al., 2016).

Macrophyte ASVs for the surfacedDNA data and the corresponding environmental parameters of the lakes were sourced from the published dataset of Stoof-Leichsenring et al. (2020). Out of the full dataset comprising 262 lakes, we selected 179 lake surface-sediment samples that contained detectable macrophyte DNA. These samples were then subjected to principal component analysis (PCA) and explanatory variables for conductivity, depth, and July temperature, which are considered important factors affecting aquatic macrophytes (Stoof-Leichsenring et al., 2022), were fitted to ordination plots. To understand the relationship between ASVs and environmental parameters in Emu Co, we projected the sedaDNA data onto the ordination diagrams constructed from surface data. A comprehensive description of these methods is available in Stoof-Leichsenring et al. (2022).

To understand the historical fluctuations in salinity within Emu Co, we developed transfer functions by utilising surface sedDNA and conductivity data from Stoof-Leichsenring et al. (2020). We employed the modern analogue technique (MAT) and weighted average partial least squares (WA-PLS) as methods for establishing the transfer function (ter Braak and Juggins, 1993; Legendre and Gallagher, 2001; Overpeck et al., 1985), with WA-PLS demonstrating superior reconstruction performance (Table 1 and Table S3). Consequently, we used the WA-PLS method to establish the sedDNA-conductivity transfer function. All 108 taxa present in the surface sedDNA data were included in the WA-PLS analysis. Considering the skewed distribution of the DNA data and the surface sediment conductivity data available, we first applied logarithmic transformation ($\log(1 + x)$) and normalisation to the resampled data. An additional square root transformation was performed to further reduce the skewness of the data during the transfer function development. The efficacy of the model was evaluated through leave-one-out cross-validation (ter Braak and Juggins, 1993), using metrics such as the coefficient of determination (R^2) for observed versus predicted values, and the root mean squared error (RMSE). To determine the optimal number of WA-PLS components, we employed a randomised *t*-test (Juggins and Birks, 2012). According to the error estimates for several calibration models, the 2-component model shows better performance than models with other numbers of components, as attested by having the highest R^2 , the lowest RMSE, and the minimal maximum bias (Table 1). The 2-component model also passed a random *t*-test with a *p*-value of 0.042. Compared to a 1-component model, the 2-component model exhibits a reduction in RMSE by more than 5% and is thus a "useful" component (Birks et al., 1998).

Table 1

Model performance statistics as assessed by "leave-one-out" cross-validation for the five components of the WA-PLS.

Method	RMSE	R^2	Ave. Bias	Max. Bias	Skill	δ .RMSE	Rand. <i>t</i> -test
Component 1	1.01	0.5991	0.04107	3.0860	59.8255	-36.6167	0.001
Component 2	0.95	0.6493	0.04865	2.8502	64.7566	-6.3379	0.042
Component 3	0.97	0.6357	0.05675	3.3120	63.1161	2.3008	0.833
Component 4	1.00	0.6160	0.04599	3.5615	60.5873	3.3713	0.873
Component 5	1.02	0.6060	0.03004	3.4228	59.2487	1.6840	0.783

RMSE = root mean squared error; Ave. Bias = Average bias; Max. Bias = Maximum bias; δ .RMSE = delta root mean squared error; Rand. *t*-test = randomisation *t*-test.

3. Results

3.1. Core lithology

Based on lithological variations including colour, texture, and sediment type (Figs. 2 and 3), the sedimentary sequence of the Emu Co core can be divided into five units (LU1-LU5).

The basal part, LU1 (387.5–360 cm; 12.6–11.8 cal ka BP), consists of brown, very coarse silt. The extremely high proportion of sand grains (34.33–45.45%, median 39.35%) affects the average grain size (29.26–38.54 μ m, median 33.24 μ m). Grain size sorting is poor in this section (3.65–3.95).

LU2 (360–196 cm; 11.8–9.5 cal ka BP) consists mainly of brown coarse silt. A decrease in the proportion of sand grains (4.35–31.16%, median 20.39%) results in a decrease in the mean grain size of LU2 (13.49–25.81 μ m, median 20.17 μ m) compared to LU1. Sorting is poor or very poor (3.05–4.20), but with a positive trend.

LU3 (196–72 cm; 9.5–4.8 cal ka BP) exhibits a gradual change in sediment colour from brown to dark yellowish brown, and a change in grain size from coarse silt-dominated to medium silt-dominated. The grain size sorting factor decreases but remains consistently poor (2.48–3.79). Occasional dark grey interlayers occur in this unit. Above 120 cm (after 8 cal. ka BP), the frequency of interlayers increases, with a notable very dark grey layer around 93 cm.

LU4 (72–68 cm; 4.8–4.7 cal ka BP) abruptly interrupts the relatively stable deposition of LU3 and is characterised by light brown coarse silt sediments approximately 4 cm thick. Grain size sorting factors (3.61–3.67) indicate deterioration in sorting.

LU5 (68–0 cm; 4.7 cal ka BP to present) consists mainly of dark brown medium silt with intermittent brown sedimentary layers, and the sorting (2.64–3.43) is generally worse than that of LU3.

3.2. Biogeochemical core composition

The lowest TOC (median 1.42%) and TN (median 0.18%) contents are found in the basal part LU1 (Fig. 3g and h). LU2 exhibits a slight increase in the TOC (1.19–3.03%, median 1.77%) and TN (0.17–0.34%, median 0.24%) values, but remains very low. High levels of TOC (median 3.52%) and TN (median 0.38%) are observed in LU3, with a peak of the TOC content (4.86%) at around 93 cm. The high levels of TOC and TN values are interrupted at LU4 and decline rapidly (median TOC 1.49% and median TN 0.19%). A downward trend is noted in LU5 with slightly lower levels of TOC (median 3.10%) and TN (median 0.33%) than in LU3. The C/N ratio is mainly below 10 in LU1 and LU2, but at about 227 cm above (after 9.7 cal ka BP) the ratio exceeds 10 (Fig. 3i). However, in the LU4 part, the C/N ratio drops below 10.

The XRF data show trends in yttrium and aluminium (Y/Al) ratios in sediment cores since 12.6 cal ka BP (Fig. 3j). The Y/Al ratios are relatively low in LU1 and LU2, then gradually increase in LU3. In LU3, the Y/Al ratio is high (median -1.91) between about 8 and 6 cal. ka BP, while significant fluctuations occur between 6 and 4.7 cal ka BP. In LU5, Y/Al values remain stable (median -2.17), slightly below the high values of 8–6 cal. ka BP, until 1 cal. ka BP when a small decrease is again observed. The Y/Al ratio increases sharply near the top of the core.

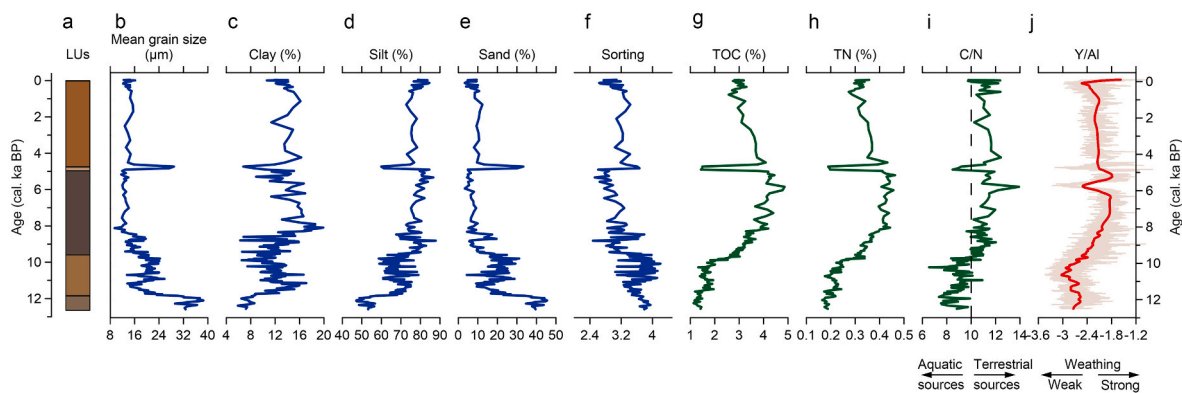


Fig. 3. Geochemical and sedimentological data from the Emu Co sediment core. (a) Lithology of Emu Co lake sediment core; (b) mean grain size, (c–e) three size fractions ($<4 \mu\text{m}$, $4\text{--}63 \mu\text{m}$, $>63 \mu\text{m}$), and (f) sorting coefficients based on Folk and Ward graphical methods (1957); (g) total organic carbon, (h) total nitrogen, and (i) C/N ratios used to determine sediment source; (j) Y/Al ratios used to track weathering levels. See Fig. 2 for details of the lithological units (LUs) of the core.

3.3. Grain-size end-member modelling

Based on sediment grain-size analysis, three robust end-members (EMs) can be discerned, all of which exhibit a bimodal distribution but with different modes (Fig. 4). EM1 contains two peaks at $7.6 \mu\text{m}$ and $111 \mu\text{m}$, both displaying broader distributions. This end-member gradually increases in proportion between 12.6 and 8 cal. ka BP and becomes dominant during the mid-Holocene. The primary peak of EM2 is situated at $35 \mu\text{m}$ (silt), accompanied by a secondary peak around $3 \mu\text{m}$ (clay), which is predominantly observed before 8 cal. ka BP and after 2 cal. ka BP. The highest grain-size peak of EM3 is $150 \mu\text{m}$ (fine sand), and the second peak is $11 \mu\text{m}$ (silt). This end-member has a high proportion until 8 cal. ka BP, after which only a sharp increase is observed at 4.8 cal. ka BP.

3.4. Aquatic macrophyte composition derived from the palynomorph analysis

The palynomorph analysis reveals two submerged macrophyte taxa (*Potamogeton* and *Myriophyllum*), two emergent macrophyte taxa (*Sparganium* and *Typha*), and the green alga *Pediastrum* (Fig. 5).

Potamogeton pollen occurs briefly at 5.7 cal ka BP, and again between 4.1 and 1 cal. ka BP, after which it disappears from the record. *Myriophyllum* pollen appears between 11 and 9 cal. ka BP, but at low concentrations (median 42 grains g^{-1}), becoming more frequent and at higher concentrations from 3.8 cal ka BP (median $158 \text{ grains g}^{-1}$). *Sparganium* and *Typha* pollen are found sporadically throughout the core. *Pediastrum* concentrations are generally low (median $10,053 \text{ grains g}^{-1}$) until ca. 5 cal. ka BP, but two peaks occur at ca. 10.3 and 8.8 cal ka BP. After 5 cal. ka BP, the *Pediastrum* concentration increases in fluctuations and reaches its maximum value ($304,632 \text{ grains g}^{-1}$) at 1.4 cal ka BP. Although the value decreases rapidly after 1.4 cal ka BP, it returns to high values in the last 100 years.

3.5. Aquatic macrophyte composition from the sedaDNA metabarcoding approach

DNA metabarcoding yielded 29 macrophyte ASVs from 62 samples, of which 19 are classified to species level and 10 to genus level (Fig. 5). Our data reveal 12 ASVs of submerged taxa and 17 emergent macrophytes. The macrophyte composition mainly consists of submerged macrophytes, including the genera *Potamogeton* (mean 43.9%) and

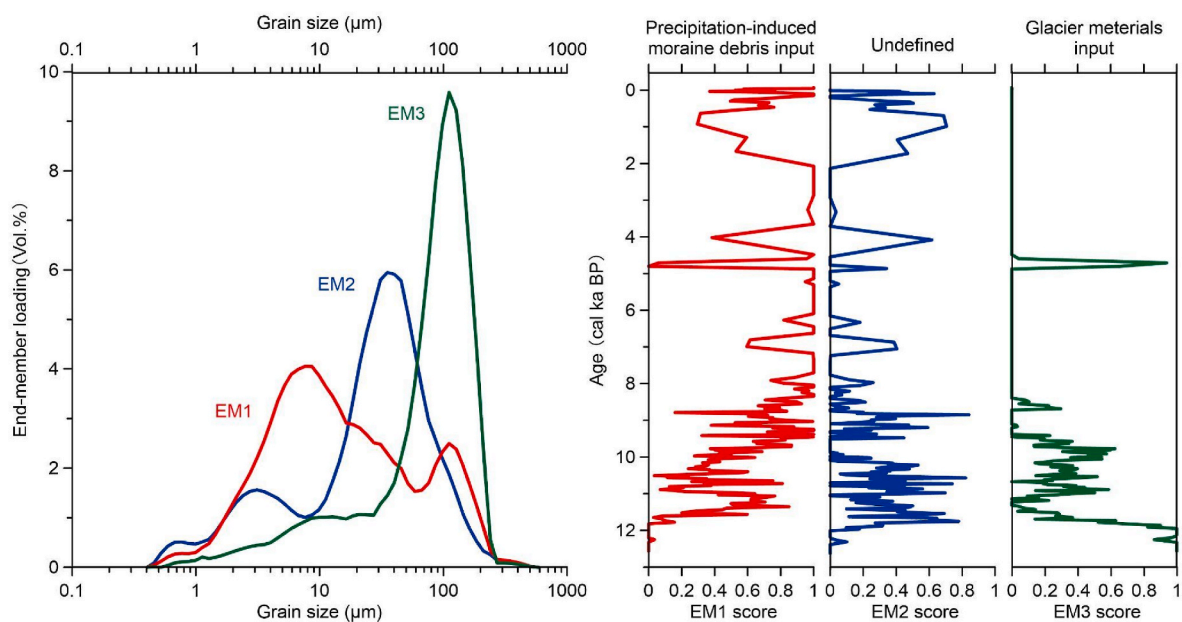


Fig. 4. Grain-size end-member modelling of the Emu Co sediment core. The three robust end-members are assumed to represent unmixed grain-size distributions from different sources to the lake basin.

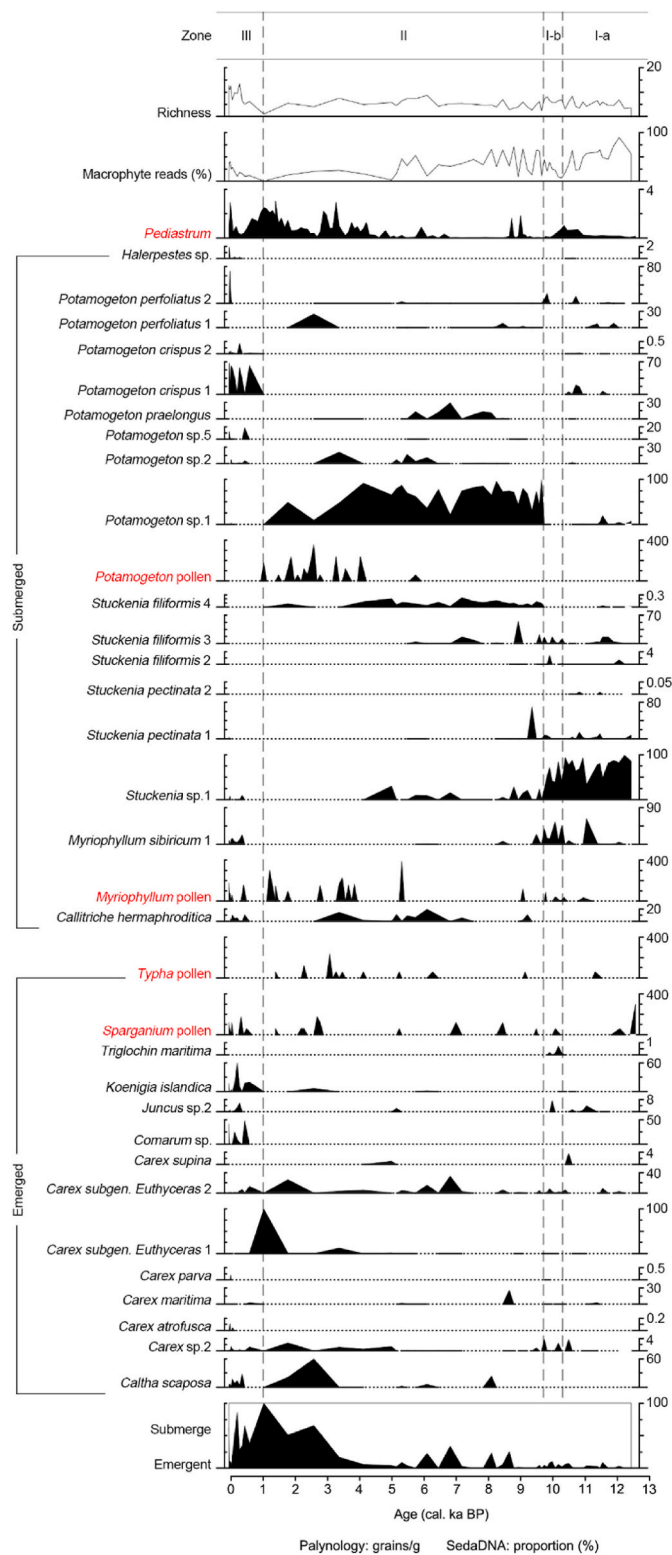


Fig. 5. Aquatic plants identified from sedaDNA and palynology (red text) in the Emu Co sediment core. Zones were determined using CONISS clustering of the sedaDNA data.

Stuckenia (mean 33.0%) from the family Potamogetonaceae and the genus *Myriophyllum* (mean 6.9%) from the family Haloragaceae. Emergent macrophytes mostly comprise the genus *Carex* from the family Cyperaceae (mean 5.7%). Based on the CONISS analysis of all aquatic macrophytes, sedaDNA records can be divided into 3 zones.

DNA Zone I (385–218 cm; 12.5–9.7 cal ka BP) is characterised by a high abundance of *Stuckenia* sp.1 (mean 68.8%) and fluctuating richness of aquatic macrophytes, ranging from 3.0 to 8.3. In DNA zone I-b (after ca. 10.3 cal ka BP), the abundance of *Stuckenia* sp.1 begins to decrease, while the frequency and abundance of *Myriophyllum sibiricum* 1 increases (mean 29.9%).

In DNA Zone II (218–51 cm; 9.7–1 cal. ka BP), *Potamogeton* sp.1 is abundant at 9.7 cal ka BP (mean 65.0%, maximum up to 99.8%), making it the dominant taxon in this zone. The abundance of *Stuckenia* sp.1 decreases, with an average of only 5.8%. Additionally, *Potamogeton praelongus* appears at 8–5 cal. ka BP (mean 10.9%), while *Callitriche hermaphroditica* occurs frequently after 7.2 cal ka BP. The richness of the macrophytes reaches a high value of 8.7 at ca. 6.1 cal ka BP, which is followed by a decrease to a few taxa.

In DNA Zone III (51–0 cm; 1 cal. ka BP to present), *Potamogeton* sp. 1 decreases and *Potamogeton crispus* 1 flourishes with high abundance (mean 35.3%). *Myriophyllum sibiricum* 1 thrives again after obscurity, averaging 7.4% abundance. *Callitriche hermaphroditica* also occurs frequently. In addition, emergent macrophytes such as *Caltha scaposa* play a more important role during this period. The richness of macrophytes increases rapidly, reaching 12.7 taxa in recent years.

3.6. SedaDNA-based conductivity reconstruction

A principal component analysis of the surface sediments run by Stooft-Leichsenring et al. (2022) reveals that the first two axes account for 34.26% of the variance in the surface sedDNA data (PCA1: 21.97%; PCA2: 12.29%; Fig. 6). When projecting the Emu Co core data onto the ordination map of surface sediments, we observe distinct patterns in the ordination diagram (Fig. 6). This distribution suggests variations in past macrophyte composition and their environmental factors. Samples from Zone I and Zone III form distinct clusters in the positive direction of PCA2, showing a strong correlation with conductivity. Conversely, samples from Zone II predominantly cluster in the negative direction of PCA2, aligning more with July temperature.

The most parsimonious two-component WA-PLS model for conductivity has an RMSE of $0.95 \mu\text{s cm}^{-1}$ ($\log(1+x)$ transformed) and an R^2 of 0.65 based on model performance statistics (Table 1). The conductivity reconstructions based on the transfer function for the upper part of

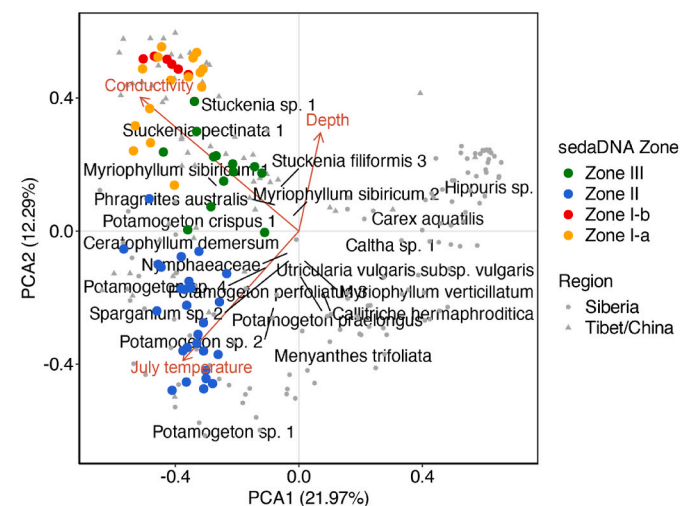


Fig. 6. PCA biplot of macrophyte taxa from surface sedDNA. Labelled taxon names are taxa explaining most of the variation. The grey dots and triangles represent sites from Siberia and Tibet/China, respectively. Surface-sediment ordination of Emu Co sediment core data and the four sedaDNA zones are distinguished by different colours. Environmental factors that account for the most significant variance in macrophyte composition are highlighted in red (Stooft-Leichsenring et al., 2022).

the core yield an average of $100.5 \mu\text{S cm}^{-1}$ across the four upper samples, while instrumental measurements are $74.5 \mu\text{S cm}^{-1}$, falling within the reconstruction error range of $36\text{--}275 \mu\text{S cm}^{-1}$ (Fig. 7). Before 8 cal. ka BP, conductivity exhibits strong fluctuations but remains generally high (ranging from 70 to $1750 \mu\text{S cm}^{-1}$, with a median of $328 \mu\text{S cm}^{-1}$). Subsequently, after 8 cal. ka BP, conductivity stabilises at lower values, with a median of $69 \mu\text{S cm}^{-1}$.

4. Discussion

4.1. Aquatic macrophyte composition and implied lake aquatic conditions

Submerged macrophytes characteristic of high conductivity lakes dominated during 12.6–9.7 cal ka BP, and lake conductivity exhibited a high variability. The continuous and substantial occurrences of the genus *Stuckenia* support a high conductivity lake habitat interpretation. Species within this genus, such as *Stuckenia pectinata* and *Stuckenia filiformis*, are submerged macrophytes with a global distribution (Van Wijk, 1988; Van Wijk et al., 1988), and are known for their positive response to moderate conductivity levels (Herzschuh et al., 2010a; Stoo-f-Leichsenring et al., 2022). A PCA of Zone I samples, which clustered in areas indicative of high conductivity, along with reconstructions of conductivity data, confirm the high lake conductivity (Figs. 6 and 7). *Stuckenia* gradually decreased after 10.4 cal ka BP and was replaced by *Myriophyllum sibiricum*, which is also a salt-tolerant taxon. Although *Myriophyllum sibiricum* is less tolerant of high salinity than *Stuckenia* sp. (Haller et al., 1974; Wang and Ji, 2007), with a slightly lower preference for high conductivity, it can still tolerate up to $900 \mu\text{S cm}^{-1}$ (Glisson and Larkin, 2021). Consequently, a decrease in lake conductivity can be inferred. In addition, the reconstructed lake conductivity deserves special emphasis as it exhibits extremely varying conditions, a variability that reflects dynamic lake salinity conditions.

The aquatic macrophytes of Emu Co were dominated by submerged freshwater taxa during 9.7–5 cal. ka BP, with the emergence of taxa associated with deep water and high nutrient levels. A major shift in macrophyte composition occurred around 9.7 cal ka BP, with *Potamogeton* sp.1 rapidly emerging as a dominant taxon, replacing salt-tolerant, high conductivity lake-specific submerged taxa. Particularly after 8 cal. ka BP, the abundance of macrophytes tolerant of high conductivity became very low (Fig. 5). This shift can also be observed in the reconstructed conductivity: the median conductivity decreased from 328 to $69 \mu\text{S cm}^{-1}$ (Fig. 7). The successive occurrences of *Potamogeton prae-longus* during 8 to 5 cal. ka BP is suggestive of clear, deep, and nutrient-rich waters, (Spence, 1967; Duigan et al., 2007). Additionally, the high macrophyte richness in the mid-Holocene also emphasises the increased nutrient levels in the lake (Rørslett, 1991).

A pronounced change from submerged to emergent taxa is observed after 5 cal. ka BP, and the growth of macrophytes appears to be constrained. *Carex* taxa, which predominantly grow in wetlands on the TP,

dominate the emergent macrophyte components during this period, possibly due to the lowering of lake levels. A decrease in lake levels can also be concluded from the increase in *Pediastrum* concentration (Jiang et al., 2013; Wu et al., 2015). There is a notable decrease in macrophyte biomass, as evidenced by the low percentage of macrophytes in total sedaDNA read counts and a declining trend in aquatic macrophyte richness (Fig. 5). Changes in the lake environment during this period can also be observed in the reproductive strategies of macrophytes. Aquatic macrophytes, including Potamogetonaceae, are capable of both autogamy and heterogamy (Philbrick, 1983). Typically, *Potamogeton* species reproduce clonally in stable environments, but sexual reproduction (i.e., pollen production) increases in fluctuating habitats (Jin and Guo, 2001; Li, 2014). This strategy helps them withstand environmental stress and maintain genetic diversity, crucial for adaptation and survival in changing conditions (Barrett et al., 1993; Harper, 1977; Jin and Guo, 2001). The increase in *Potamogeton* pollen counts between 4.1 cal ka BP and 1 cal. ka BP may indicate suboptimal conditions in the lake for these taxa (Fig. 5).

Another significant transformation in the composition of macrophytes occurred after 1 cal. ka BP, characterised by the emergence of taxa associated with nutrient-rich waters. The rapid increase in the abundance of *Potamogeton crispus* and richness imply changes in lake nutrient levels. *Potamogeton crispus* is known to be associated with nutrient-enriched water bodies (Nichols and Shaw, 1986; Bolduan et al., 1994), flourishing in many eutrophic lakes in China (Zhang et al., 2022). The increased macrophyte richness observed in once nutrient-poor TP lakes can be attributed to enhanced nutrient conditions in the waters (Li et al., 2018).

4.2. Potential drivers of past changes in aquatic macrophytes and lake water condition

4.2.1. 12.6–9.7 cal ka BP

Our data indicate that glacial melt during early-Holocene warming strongly impacted the hydrology of Emu Co. Previous studies have suggested that higher summer insolation (Fig. 8a; Laskar et al., 2004) during the early Holocene led to increased evaporation and insufficient effective moisture in the eastern TP (e.g., Mischke et al., 2007; 2010; Qiang et al., 2016), which could explain the higher conductivity of lakes in the region during this period. However, rapid early-Holocene warming under the influence of higher summer insolation would have induced the ablation of the Nianbaoyuze glacier (Fig. 8b; Marcott et al., 2013; Herzschuh et al., 2014), which recharged Emu Co. The importance of fluvial processes for sediment transport over the catchment increased as glaciers retreated from the lake basin (Zhang and Mischke, 2009). This is confirmed by reductions in mean grain size and sand proportions as well as improved grain-size sorting (Fig. 3b–e, f). The bimodal distribution of EM3 scarcely overlaps, highlighting the fundamental characteristics typical of fluvial sediments, and we therefore interpret EM3 as an input of upstream glacial material. Declines in fluctuating EM3 scores are indicative of glacial melting in the early Holocene (Fig. 8c). In addition, high sedimentation rates and low TOC values (Figs. 2 and 3g) emphasise the important, albeit diminishing, role of glacial meltwater (Hallet et al., 1996; Leonard, 1997; Loso et al., 2004). In general, the solute content in glacier surface meltwater was remarkably low, registering conductivities of only $2.7\text{--}5.4 \mu\text{S cm}^{-1}$ (Collins, 1979). From 12.6 cal ka BP to the early Holocene, the influx of glacial meltwater, with very low ionic content, flowed into the Emu Co basin, inevitably lowering lake conductivity.

Besides glacial meltwater, increased precipitation in the early Holocene played a positive role in reducing the conductivity of Emu Co. Following the glacial retreat near Emu Co, extensive moraines were formed around the lake (Lehmkuhl and Liu, 1994), and debris from these moraines would enter the lake through slope runoff after weathering. The bimodal structure of EM1 aligns with grain size distributions of other glacial detrital materials (Fig. 4; Weltje and Prins, 2007; Liu

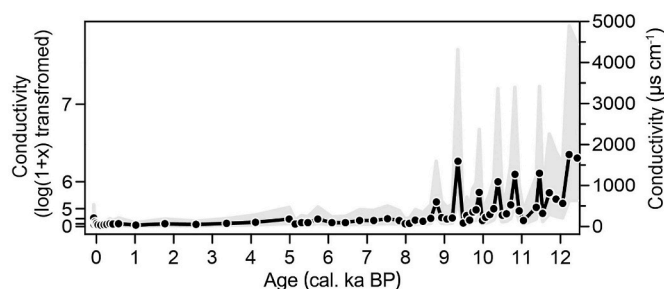


Fig. 7. Reconstruction of Emu Co conductivity based on sedaDNA-identified macrophytes using WA-PLS. The left axis is conductivity after a $\log(1+x)$ transformation. The right-hand axis is the reverse transformed reconstructed conductivity. Shading denotes one standard deviation of the reconstructed conductivity.

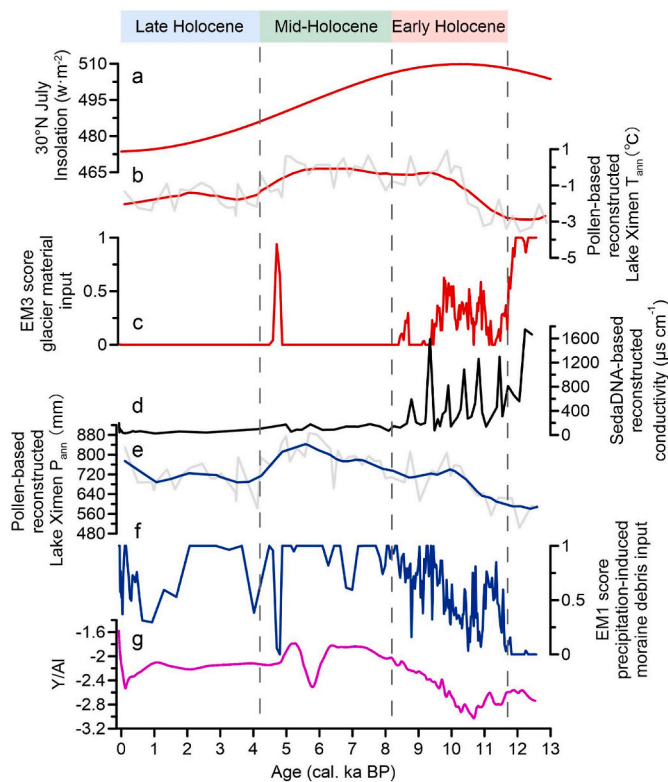


Fig. 8. Comparison of temperature and precipitation change in the Nianbaoyuze area with catchment changes. (a) 30°N July insolation (Laskar et al., 2004); (b) pollen-based annual temperature (T_{ann}) reconstructions from Lake Ximen (Herzschuh et al., 2014); (c) EM3 score representing glacier material input (this study); (d) sedaDNA-based conductivity reconstructions from Emu Co (this study); (e) pollen-based annual precipitation (P_{ann}) reconstructions from Lake Ximen (Herzschuh et al., 2014); (f) EM1 score representing precipitation-induced moraine debris input (this study); (g) weathering indicator Y/Al ratio (this study).

et al., 2010; Zhang et al., 2023). Hence, the magnitude of EM1 scores depends on the migration of debris from lakeshore moraines, offering a benchmark to assess the intensity of regional precipitation. The EM1 scores fluctuate with an increasing trend from the beginning of our record to the early Holocene, indicating the growing influence of atmospheric precipitation on Emu Co (Fig. 4). This inference is supported by changes in precipitation inferred from pollen data within the lake (Li et al., 2023) and the neighbouring Ximen Co (Fig. 8e; Herzschuh et al., 2014). Additionally, the increase in Y/Al values during this period may be related to increased weathering (Fig. 3j). This is because element Y is thought to be more soluble and mobile, derived from chemical weathering and abundant precipitation, whereas Al is thought to be more insoluble and resistant (Mackereth, 1966; Zhong et al., 2012; Mischke and Zhang, 2010). The salinity of atmospheric precipitation is nearly zero upon initial contact with the surface, indicating very low ionic content that increases only after interaction with carbonate rocks (Meng et al., 2013). Geological studies reveal the absence of carbonate rock development in the Nianbaoyuze area (Zhang and Mischke, 2009; China Geological Survey Chengdu Center, 2013). Hence, it can be reasonably inferred that the influx of precipitation via overland flow lowers the conductivity of Emu Co.

Climatic instability during the early Holocene explains the strong fluctuations in lake conductivity during this time. Studies have indicated early Holocene climate instability in the TP, marked by cold events (Mischke and Zhang, 2010). Rapid fluctuations in our glacier ablation proxies imply that glacial meltwater inputs are not stable, with short-term meltwater pulses occurring during periods of rapid glacial

melt (Fig. 8d). Additionally, the East Asian monsoon system was unstable during the late Pleistocene to early Holocene (Zhao et al., 2023; Pang et al., 2024), affecting precipitation indicators (Fig. 8f). High evaporation rates may initially have led Emu Co's conductivity to increase, but it started to decrease with warming and humidification. However, pulses of freshwater dominated by glacial meltwater resulted in significant conductivity fluctuations within this decreasing trend.

4.2.2. 9.7–1 cal. ka BP

Stable lake-recharge conditions and warm and moist climatic conditions created an ideal environment for aquatic macrophytes in Emu Co during the mid-Holocene (8–5 cal. ka BP). The decline in sedimentation rates coupled with the rapid rise in TOC values after 9.7 cal. ka BP indicate a reduction in glacial influence on the lake (Figs. 2 and 3; Hicks et al., 1990; Hallet, 1996; Leonard, 1997; Loso et al., 2004). After 8 cal. ka BP, the input of glacial material by meltwater stopped and the lake conditions stabilised. By this time, lake conductivity reached and maintained a low value of $\sim 70 \mu\text{S cm}^{-1}$ (Fig. 8d). Numerous studies have indicated that the Holocene climatic optimum on the TP (Mischke et al., 2010; Zhao et al., 2011; Chen et al., 2020), a period of warmer and wetter conditions, occurred during the mid-Holocene. The Emu Co region followed this climatic trend, as reflected by the high value of our weathering proxy Y/Al (Fig. 8g). EM1 scores and precipitation reconstructions based on pollen data suggest that high precipitation (pollen reconstructed >700 mm, which is higher than current precipitation) in the Nianbaoyuze area starting at ca. 10 cal. ka BP continued until about 5 cal. ka BP before showing a downward trend (Fig. 8e and f; Herzschuh et al., 2014; Li et al., 2023). This stable freshwater recharge likely maintained low conductivity and high water level in Emu Co, fostering a suitable freshwater habitat for aquatic macrophytes. High-temperature conditions not only promoted the growth of warmth-loving aquatic macrophytes, such as *Callitriche hermaphroditica* (Väliranta et al., 2015), but also induced the expansion of terrestrial vegetation around the lake (Li et al., 2023). The increased nutrient supply from terrestrial sources, entering the lake through runoff, could have enhanced macrophyte richness in Emu Co, particularly in a context of relatively low nutrient levels in the lake (Rørslett, 1991). The C/N ratio exceeds 10 after 9.7 cal. ka BP underscoring the significant terrestrial influence on the lake ecosystem (Meyers, 2003). Our PCA results also show the effects of high July temperatures on lake macrophyte composition (Fig. 6).

Cold and arid climatic conditions during the mid-to-late Holocene disrupted the deep-water, nutrient-appropriate, favourable lake environment of Emu Co. Despite the absence of corresponding signals in the sedaDNA data, likely due to sample precision limitations, both the geochemical and sedimentological proxies in Emu Co register significant changes around 4.8 cal. ka BP (Fig. 3). Studies from the TP suggest that around 5 cal. ka BP a climatic transition occurred on the TP (Herzschuh et al., 2006; Ning et al., 2022), and for the eastern part of the TP many records transition from warm and wet to cold and dry (Li et al., 2023). Therefore, this abrupt change may be related to a regional event in the catchment during the climatic transition. Following this event, the Emu Co regional climate and lake environment changed. TOC values, indicative of terrestrial and aquatic plant biomass in the basin, along with TN values, reflecting lake nutrient status, show a continuous decline (Fig. 3g and h; Håkanson and Jansson, 1983; Meyers, 2003). There is also a slight increase in the coarse-grained sediment component associated with glacier activity (Fig. 3b and e), and the sorting trend that began in the early Holocene appears to reverse (Fig. 3f). These changes are likely a response to the colder, drier climatic conditions and a late Holocene glacier advance (Liu et al., 2014; Solomina et al., 2015). The cold and dry climate not only led to a transition of terrestrial vegetation from forests to meadows (Li et al., 2023), but may also have caused a reduction in the biomass of aquatic macrophytes by lowering water level and temperatures, shortening the growing season, and reducing nutrient inputs.

4.2.3. 1 cal. ka BP to present

The shift in aquatic macrophyte composition in Emu Co during the past thousand years can be attributed to human-induced changes by impacting lake nutrient levels. While some studies have indicated a long history of human activities in the Nianbaoyuzhe area (Schlütz and Lehmkuhl, 2009; Herzsuh et al., 2014), dating back to as early as 7.2 cal ka BP, the examination of pollen data from Emu Co does not reveal a similar long-term signal. We observed only a slight increase in pollen types associated with grazing indicators such as Asteraceae, *Trollius*, and Cichoriodeae around 1 cal. ka BP (Schlütz and Lehmkuhl, 2009; Li et al., 2023). This modest change, potentially attributable to livestock grazing, is corroborated by a 600-year pollen record from Dongerwuka Lake, located upstream of Emu Co (Wischniewski et al., 2014). These human influences, particularly livestock grazing, likely led to the introduction of nutrients into the lake, as reflected in the increased TN and TOC content in the sediments (Fig. 3 g and h).

While the predictive ability of our transfer function ($R^2 = 0.65$) slightly lags behind those based on ostracod ($R^2 = 0.71$; Mischke et al., 2007) and diatom ($R^2 = 0.92$; Yang et al., 2003) data, the sedaDNA method effectively overcomes the limitations of traditional methods with respect to accessibility, resolution, and identification standards. Our sedaDNA-based conductivity transfer function offers a new, reliable means of quantitatively reconstructing changes in lake conductivity. Moreover, we anticipate that the predictive accuracy of the sedaDNA-based transfer function can be enhanced with the publication of additional surface sedaDNA data.

5. Conclusions

In this study, we used sedaDNA metabarcoding and palynology to chart the history of aquatic plants in Emu Co for the period from 12.6 cal ka BP to the present, developed a model to follow Holocene conductivity variation, and investigated catchment impacts on aquatic conditions of the lake and the composition of the aquatic macrophytes through physical and chemical proxies. The period from 12.6 to 9.7 cal ka BP was a time of high conductivity in the lake due to high evaporation, but temporally high inputs of glacial meltwater and freshwater recharge from precipitation reduced the conductivity of the lake, eventually leading to a decrease in the dominance of taxa characterised by high conductivity. Climate instability-induced pulses of freshwater explains the strong fluctuations in lake conductivity during the early Holocene. After 8 cal. ka BP, the development of freshwater taxa was further catalysed by a warmer and wetter climate and stable lake-water conditions. After 5 cal. ka BP, cold and arid climatic conditions led to a decline in lake levels which resulted in a macrophyte richness decline. Furthermore, we assume that sub-optimal conditions for macrophyte growth supported a shift from an asexual to a sexual reproductive strategy. Since 1 cal. ka BP, macrophytes that can take advantage of nutrient-rich waters flourished, likely reflecting an increase in human activities.

Author contributions

All authors have made substantial contributions to the manuscript. U.H. and W.L. designed the study. U.H., X.C. and W.L. led the interpretation and writing. W.L. wrote the first draft of the manuscript. X.C. contributed to the core collection and W.L. performed lab work. W.L., K.R.S., X.H., S.-Y. Y. and F. T. implemented the data analysis and statistical analyses. All authors discussed the results and provided intellectual input to the manuscript.

Declaration of competing interest

The authors declare that they have no known competing financial interests or personal relationships that could have appeared to influence the work reported in this paper.

Data availability

DNA sequence data from this study have been deposited in the European Nucleotide Archive (ENA) under accession number PRJEB74743 (<https://www.ebi.ac.uk/ena/data/view/PRJEB74743>). The tag files required to identify the samples in the two libraries are provided in the Supplementary file. Geochemical, sedimentological, and palaeontological data will be made available upon request.

Acknowledgements

We would like to express our gratitude to the editor Dr. Patrick Rioual, reviewer Dr. Anders Schomacker and one anonymous reviewer in strengthening this paper with their valuable feedback. Also, thanks are due to Yangrong Zhang and Nannan Wang for help during fieldwork, to Ying Liu, Iris Eder, Sarah Olischläger and Janine Klimke for their technical support in the paleogenetic laboratories, to Shaopeng Gao for his technical support in ITRAX XRF core scanning, to Wei Shen and Sisi Liu for their help in sedaDNA data analysis. Helpful comments concerning elemental interpretation were provided by Weihai Jia. Cathy Jenks provided help with language editing. This research was supported by the National Natural Science Foundation of China (Grant No. 42071107), the Chinesisch-Deutsches Mobilitätsprogramm (project No. M-0359), and the China Scholarship Council (CSC, Grant No. 202204910401 to WJ.L.).

Appendix A. Supplementary data

Supplementary data to this article can be found online at <https://doi.org/10.1016/j.quascirev.2024.108806>.

References

- Alsos, I.G., Lammers, Y., Yoccoz, N.G., Jørgensen, T., Sjögren, P., Gielly, L., Edwards, M. E., 2018. Plant DNA metabarcoding of lake sediments: how does it represent the contemporary vegetation. *PLoS One* 13, e0195403. <https://doi.org/10.1371/journal.pone.0195403>.
- Alsos, I.G., Rijal, D.P., Ehrich, D., Karger, D.N., Yoccoz, N.G., Heintzman, P.D., Brown, A. G., Lammers, Y., Pellissier, L., Alm, T., Bråthen, K.A., Coissac, E., Merkel, M.K.F., Alberti, A., Denoed, F., Bakke, J., PhyloNorway Consortium, 2022. Postglacial species arrival and diversity buildup of northern ecosystems took millennia. *Sci. Adv.* 8, eabo7434 <https://doi.org/10.1126/sciadv.abo7434>.
- Baishева, I., Pstryakova, L., Levina, S., Glückler, R., Biskaborn, B.K., Vyse, S.A., Heim, B., Herzsuh, U., Stoof-Leichsenring, K.R., 2023. Permafrost-thaw lake development in Central Yakutia: sedimentary ancient DNA and element analyses from a Holocene sediment record. *J. Paleolimnol.* 70, 95–112. <https://doi.org/10.1007/s10933-023-00285-w>.
- Barrett, S.C., Eckert, C.G., Husband, B.C., 1993. Evolutionary processes in aquatic plant populations. *Aquat. Bot.* 44, 105–145. [https://doi.org/10.1016/0304-3770\(93\)90068-8](https://doi.org/10.1016/0304-3770(93)90068-8).
- Birks, H.H., 2001. Plant macrofossils. In: Smol, J.P., Birks, H.J.B., Last, W.M., Bradley, R. S., Alverson, K. (Eds.), *Tracking Environmental Change Using Lake Sediments: Terrestrial, Algal, and Siliceous Indicators, Developments in Paleoenvironmental Research*. Springer, Netherlands, Dordrecht, pp. 49–74. https://doi.org/10.1007/0-306-47668-1_4.
- Birks, H.H., Birks, H.J.B., 2000. Future uses of pollen analysis must include plant macrofossils. *J. Biogeogr.* 27, 31–35.
- Birks, H.J.B., Birks, H.H., 2016. How have studies of ancient DNA from sediments contributed to the reconstruction of Quaternary floras? *New Phytol.* 209, 499–506. <https://doi.org/10.1111/nph.13657>.
- Birks, H.J.B., 1998. Numerical tools in palaeolimnology-progress, potentialities, and problems. *J. Paleolimnol.* 20, 307–332. <https://doi.org/10.1023/A:1008038808690>.
- Blott, S.J., Pye, K., 2001. GRADISTAT: a grain size distribution and statistics package for the analysis of unconsolidated sediments. *Earth Surf. Process. Landforms* 26, 1237–1248. <https://doi.org/10.1002/esp.261>.
- Bolduan, B.R., Van Eeckhout, G.C., Quade, H.W., Gannon, J.E., 1994. *Potamogeton crispus* – the other invader. *Lake Reserv. Manag.* 10, 113–125. <https://doi.org/10.1080/07438149409354182>.
- Boyer, F., Mercier, C., Bonin, A., Le Bras, Y., Taberlet, P., Coissac, E., 2016. obitools: a unix-inspired software package for DNA metabarcoding. *Mol. Ecol. Resour.* 16, 176–182. <https://doi.org/10.1111/1755-0998.12428>.
- Cao, X., Tian, F., Li, K., Ni, J., 2021. Atlas of pollen and spores for common plants from the east Tibetan Plateau. *Natl. Tibet. Plateau Data Cent.* <https://doi.org/10.11888/Paleoenv.tpdc.271191>.

- Capo, E., Giguët-Covex, C., Rouillard, A., Nota, K., Heintzman, P.D., Vuillemin, A., Ariztegui, D., Arnaud, F., Belle, S., Bertilsson, S., Bigler, C., Bindler, R., Brown, A.G., Clarke, C.L., Crump, S.E., Debroas, D., Englund, G., Ficotola, G.F., Garner, R.E., Gauthier, J., Gregory-Eaves, I., Heinecke, L., Herzschuh, U., Ibrahim, A., Kisan, V., Kjær, K.H., Lammers, Y., Littlefair, J., Messenger, E., Monchamp, M.-E., Olajos, F., Orsi, W., Pedersen, M.W., Rijal, D.P., Rydberg, J., Spanbauer, T., Stooft-Leichsenring, K.R., Taberlet, P., Talas, L., Thomas, C., Walsh, D.A., Wang, Y., Willerslev, E., van Woerkom, A., Zimmermann, H.H., Coolen, M.J.L., Epp, L.S., Domaizon, I., G. Alsos, I., Parducci, L., 2021. Lake sedimentary DNA research on past terrestrial and aquatic biodiversity: overview and recommendations. *Quaternary* 4, 6. <https://doi.org/10.3390/quat4010006>.
- Chambers, P.A., Lacoul, P., Murphy, K.J., Thomaz, S.M., 2008. Global diversity of aquatic macrophytes in freshwater. In: Balian, E.V., Lévêque, C., Segers, H., Martens, K. (Eds.), *Freshwater Animal Diversity Assessment, Developments in Hydrobiology*. Springer, Netherlands, Dordrecht, pp. 9–26. https://doi.org/10.1007/978-1-4020-8259-7_2.
- Chen, F., Zhang, J., Liu, J., Cao, X., Hou, J., Zhu, L., Xu, X., Liu, X., Wang, M., Wu, D., Huang, L., Zeng, T., Zhang, S., Huang, W., Zhang, X., Yang, K., 2020. Climate change, vegetation history, and landscape responses on the Tibetan Plateau during the Holocene: a comprehensive review. *Quat. Sci. Rev.* 243, 106444 <https://doi.org/10.1016/j.quascirev.2020.106444>.
- China Geological Survey Chengdu Center, 2013. *Geological map of Tibetan Plateau and its surrounding areas*. 1:1,500,000. Geological Publishing House, Beijing.
- Coissac, E., Riaz, T., Puillandre, N., 2012. Bioinformatic challenges for DNA metabarcoding of plants and animals. *Mol. Ecol.* 21, 1834–1847. <https://doi.org/10.1111/j.1365-294X.2012.05550.x>.
- Croudace, I.W., Rothwell, R.G., 2015. *Micro-XRF Studies of Sediment Cores: Applications of a Non-destructive Tool for the Environmental Sciences*. Springer, Dordrecht. <https://doi.org/10.1007/978-94-017-9849-5>.
- Collins, D.N., 1979. Hydrochemistry of meltwaters draining from an alpine glacier. *Arct. Alp. Res.* 307–324. <https://doi.org/10.1080/00040851.1979.12004139>.
- De Barba, M., Adams, J.R., Goldberg, C.S., Stansbury, C.R., Arias, D., Cisneros, R., Waits, L.P., 2014. Molecular species identification for multiple carnivores. *Conserv. Genet. Resour.* 6, 821–824. <https://doi.org/10.1007/s12686-014-0257-x>.
- Dietze, E., Hartmann, K., Diekmann, B., Jmker, J., Lehmküh, F., Opitz, S., Stauch, G., Wünnemann, B., Borchers, A., 2012. An end-member algorithm for deciphering modern detrital processes from lake sediments of Lake Donggi Cona, NE Tibetan Plateau, China. *Sediment. Geol.* 243–244, 169–180. <https://doi.org/10.1016/j.sedgeo.2011.09.014>.
- Duigan, C., Kovach, W., Palmer, M., 2007. Vegetation communities of British lakes: a revised classification scheme for conservation. *Aquat. Conserv. Mar. Freshw. Ecosyst.* 17, 147–173. <https://doi.org/10.1002/aq.780>.
- Faegri, K., Iversen, J., Kaland, P.E., Krzywinski, K., 1989. *Textbook of Pollen Analysis*, fourth ed. John Wiley & Sons Ltd.
- Folk, R.L., Ward, W.C., 1957. Brazos River bar [Texas]; a study in the significance of grain size parameters. *J. Sediment. Res.* 27, 3–26. <https://doi.org/10.1306/74D70646-2B21-11D7-8648000102C1865D>.
- Ge, Y., Zhang, K., Yang, X., 2018. Long-term succession of aquatic plants reconstructed from palynological records in a shallow freshwater lake. *Sci. Total Environ.* 643, 312–323. <https://doi.org/10.1016/j.scitotenv.2018.06.203>.
- Gibbs, R.J., 1970. Mechanisms controlling world water chemistry. *Science* 170, 1088–1090. <https://doi.org/10.1126/science.170.3962.1088>.
- Glisson, W.J., Larkin, D.J., 2021. Phenology Data for Watermillfoil Taxa *Myriophyllum Spicatum*, M. *Sibiricum*, and M. *Spicatum* X M. *Sibiricum* in Minnesota, USA, 2017–2018. Data Repository for the University of Minnesota. doi: 10.13020/5xq3-wb66.
- Grimm, E.C., 1987. CONISS: a FORTRAN 77 program for stratigraphically constrained cluster analysis by the method of incremental sum of squares. *Comput. Geosci.* 13, 13–35. [https://doi.org/10.1016/0098-3004\(87\)90022-7](https://doi.org/10.1016/0098-3004(87)90022-7).
- Håkanson, L., Jansson, M., 1983. *Principles of Lake Sedimentology*. Springer-verlag Berlin.
- Haller, W.T., Sutton, D.L., Barlowe, W.C., 1974. Effects of salinity on growth of several aquatic macrophytes. *Ecology* 55, 891–894. <https://doi.org/10.2307/1934427>.
- Hallet, B., 1996. Glacial quarrying: a simple theoretical model. *Ann. Glaciol.* 22, 1–8. <https://doi.org/10.3189/1996Aog22-1-1-8>.
- Hallet, B., Hunter, L., Bogen, J., 1996. Rates of erosion and sediment evacuation by glaciers: a review of field data and their implications. *Glob. Planet. Change* 12, 213–235. [https://doi.org/10.1016/0921-8181\(95\)00021-6](https://doi.org/10.1016/0921-8181(95)00021-6).
- Han, W., Zhang, E., Sun, W., Lin, Q., Meng, X., Ni, Z., Ning, D., Shen, J., 2023. Anthropogenic activities altering the ecosystem in lake Yamzhog Yumco, southern Qinghai-Tibetan plateau. *Sci. Total Environ.* 904, 166715 <https://doi.org/10.1016/j.scitotenv.2023.166715>.
- Harper, J.L., 1977. *Population Biology of Plants*. Academic Press.
- Herzschuh, U., Borkowski, J., Schewe, J., Mischke, S., Tian, F., 2014. Moisture-advection feedback supports strong early-to-mid Holocene monsoon climate on the eastern Tibetan Plateau as inferred from a pollen-based reconstruction. *Palaeogeogr. Palaeoclimatol. Palaeoecol.* 402, 44–54. <https://doi.org/10.1016/j.palaeo.2014.02.022>.
- Herzschuh, U., Mischke, S., Meyer, H., Plessen, B., Zhang, C., 2010a. Using variations in the stable carbon isotope composition of macrophyte remains to quantify nutrient dynamics in lakes. *J. Paleolimnol.* 43, 739–750. <https://doi.org/10.1007/s10933-009-9365-0>.
- Herzschuh, U., Mischke, S., Meyer, H., Plessen, B., Zhang, C., 2010b. Lake nutrient variability inferred from elemental (C, N, S) and isotopic ($\delta^{13}\text{C}$, $\delta^{15}\text{N}$) analyses of aquatic plant macrofossils. *Quat. Sci. Rev.* 29, 2161–2172. <https://doi.org/10.1016/j.quascirev.2010.05.011>.
- Herzschuh, U., Winter, K., Wünnemann, B., Li, S., 2006. A general cooling trend on the central Tibetan Plateau throughout the Holocene recorded by the Lake Zigetang pollen spectra. *Quat. Int.* 154, 113–121. <https://doi.org/10.1016/j.quaint.2006.02.005>.
- Hicks, D.M., McSaveney, M.J., Chinn, T.J.H., 1990. Sedimentation in proglacial Ivory lake, southern Alps, New Zealand. *Arct. Alp. Res.* 26–42. <https://doi.org/10.2307/1551718>.
- Hou, J., D'Andrea, W.J., Liu, Z., 2012. The influence of ^{14}C reservoir age on interpretation of paleolimnological records from the Tibetan Plateau. *Quat. Sci. Rev.* 48, 67–79. <https://doi.org/10.1016/j.quascirev.2012.06.008>.
- Hsieh, T.C., Ma, K.H., Chao, A., 2016. iNEXT: an R package for rarefaction and extrapolation of species diversity (Hill numbers). *Methods Ecol. Evol.* 7, 1451–1456. <https://doi.org/10.1111/2041-210X.12613>.
- Immerzeel, W.W., van Beek, L.P.H., Bierkens, M.F.P., 2010. Climate change will affect the Asian water towers. *Science* 328, 1382–1385. <https://doi.org/10.1126/science.1183188>.
- James, W.F., 2008. Effects of lime-induced inorganic carbon reduction on the growth of three aquatic macrophyte species. *Aquat. Bot.* 88, 99–104. <https://doi.org/10.1016/j.aquabot.2007.08.011>.
- Jiang, Q., Ji, J., Shen, J., Matsumoto, R., Tong, G., Qian, P., Ren, X., Yan, D., 2013. Holocene vegetational and climatic variation in westerly-dominated areas of Central Asia inferred from the Sayram Lake in northern Xinjiang, China. *Sci. China Earth Sci.* 56, 339–353. <https://doi.org/10.1007/s11430-012-4550-9>.
- Jin, B., Guo, Y., 2001. Primary studies on the reproductive characteristics of *Potamogeton maackianus*. *Acta Hydrobiol. Sin.* 25, 439–448.
- Juggins, S., Birks, H.J.B., 2012. Quantitative environmental reconstructions from biological data. In: Birks, H.J.B., Lotter, A.F., Juggins, S., Smol, J.P. (Eds.), *Tracking Environmental Change Using Lake Sediments, Vol. 5: Numerical and Data Handling Techniques*. Springer, Netherlands, Dordrecht, pp. 431–494. https://doi.org/10.1007/978-94-007-2745-8_14.
- Karachurina, S., Rudaya, N., Frolova, L., Kuzmina, O., Cao, X., Chepinoga, V., Stooft-Leichsenring, K., Biskaborn, B., Herzschuh, U., Nigmatullin, N., 2023. Terrestrial vegetation and lake aquatic community diversity under climate change during the mid-late Holocene in the Altai Mountains. *Palaeogeogr. Palaeoclimatol. Palaeoecol.* 623, 111623. <https://doi.org/10.1016/j.palaeo.2023.111623>.
- Laskar, J., Robutel, P., Joutel, F., Gastineau, M., Correia, A.C.M., Levrard, B., 2004. A long-term numerical solution for the insolation quantities of the Earth. *Astron. Astrophys.* 428, 261–285. <https://doi.org/10.1051/0004-6361:20041335>.
- Legendre, P., Gallagher, E.D., 2001. Ecologically meaningful transformations for ordination of species data. *Oecologia* 129, 271–280. <https://doi.org/10.1007/s004420100716>.
- Lehmkuhl, F., 1998. Extent and spatial distribution of Pleistocene glaciations in eastern Tibet. *Quat. Int.* 45–46, 123–134. [https://doi.org/10.1016/S1040-6182\(97\)00010-4](https://doi.org/10.1016/S1040-6182(97)00010-4).
- Lehmkuhl, F., Liu, S., 1994. An outline of physical geography including Pleistocene glacial landforms of Eastern Tibet (provinces Sichuan and Qinghai). *Geojournal* 34, 7–30. <https://doi.org/10.1007/BF00813966>.
- Leonard, E.M., 1997. The relationship between glacial activity and sediment production: evidence from a 4450-year varve record of neoglaciation in Hector Lake, Alberta, Canada. *J. Paleolimnol.* 17, 319–330. <https://doi.org/10.1023/A:1007948327654>.
- Li, K., Stooft-Leichsenring, K.R., Liu, S., Jia, W., Liao, M., Liu, X., Ni, J., Herzschuh, U., 2021. Plant sedimentary DNA as a proxy for vegetation reconstruction in eastern and northern Asia. *Ecol. Indic.* 132, 108303 <https://doi.org/10.1016/j.ecolind.2021.108303>.
- Li, N., Li, J.-X., Li, G.-W., Li, Y., Xi, B.-D., Wu, Y.-W., Li, C.-L., Li, W., Zhang, L.-Y., 2018. The eutrophication and its regional heterogeneity in typical lakes of China. *Acta Hydrobiol. Sin.* 42, 854–864. <https://doi.org/10.7541/2018.105>.
- Li, W., 2014. Environmental opportunities and constraints in the reproduction and dispersal of aquatic plants. *Aquat. Bot.* 118, 62–70. <https://doi.org/10.1016/j.aquabot.2014.07.008>.
- Li, W., Wang, N., Liang, C., Yu, S., Tian, F., Cao, X., 2023. Regional peculiarities in the importance of precipitation and temperature on mid-to-late Holocene arboreal degradation on the eastern Tibetan Plateau. *Glob. Planet. Change* 229, 104252. <https://doi.org/10.1016/j.gloplacha.2023.104252>.
- Liu, S., Kruse, S., Scherler, D., Ree, R.H., Zimmermann, H.H., Stooft-Leichsenring, K.R., Epp, L.S., Mischke, S., Herzschuh, U., 2021a. Sedimentary ancient DNA reveals a threat of warming-induced alpine habitat loss to Tibetan Plateau plant diversity. *Nat. Commun.* 12, 2995. <https://doi.org/10.1038/s41467-021-22986-4>.
- Liu, S., Li, K., Jia, W., Stooft-Leichsenring, K.R., Liu, X., Cao, X., Herzschuh, U., 2021b. Vegetation reconstruction from Siberia and the Tibetan Plateau using modern analogue technique – comparing sedimentary (ancient) DNA and pollen data. *Front. Ecol. Evol.* 9 <https://doi.org/10.3389/fevo.2021.668611>.
- Liu, X., Herzschuh, U., Wang, Y., Kuhn, G., Yu, Z., 2014. Glacier fluctuations of Muztagh Ata and temperature changes during the late Holocene in westernmost Tibetan Plateau, based on glaciolacustrine sediment records. *Geophys. Res. Lett.* 41, 6265–6273. <https://doi.org/10.1002/2014GL060444>.
- Liu, X., Yao, B., Yang, B., 2010. Grain size distribution of aeolian and lacustrine sediments of Kusai lake in the Hoh Xil region of the northern Qinghai-Tibetan plateau. *Quat. Sci.* 30, 1193–1198.
- Loso, M.G., Anderson, R.S., Anderson, S.P., 2004. Post-Little Ice Age record of coarse and fine clastic sedimentation in an Alaskan proglacial lake. *Geology* 32, 1065–1068. <https://doi.org/10.1130/G20839.1>.
- Ma, R., Duan, H., Hu, C., Feng, X., Li, A., Ju, W., Jiang, J., Yang, G., 2010. A half-century of changes in China's lakes: global warming or human influence? *Geophys. Res. Lett.* 37 <https://doi.org/10.1029/2010GL045514>.

- Mackereth, F.J., 1966. Some chemical observations on post-glacial lake sediments. *Philosophical Transactions of the Royal Society of London. Series B, Biological Sciences* 250, 165–213. <https://doi.org/10.1098/rstb.1966.0001>.
- Marcott, S.A., Shakun, J.D., Clark, P.U., Mix, A.C., 2013. A reconstruction of regional and global temperature for the past 11,300 years. *Science* 339, 1198–1201. <https://doi.org/10.1126/science.1228026>.
- Meng, Q., Zhu, D., Hu, W., Jin, Z., 2013. Dissolution-filling mechanism of atmospheric precipitation controlled by both thermodynamics and kinetics. *Sci. China Earth Sci.* 56, 2150–2159. <https://doi.org/10.1007/s11430-013-4711-5>.
- Meyers, P.A., 2003. Applications of organic geochemistry to paleolimnological reconstructions: a summary of examples from the Laurentian Great Lakes. *Org. Geochem.* 34, 261–289. [https://doi.org/10.1016/S0146-6380\(02\)00168-7](https://doi.org/10.1016/S0146-6380(02)00168-7).
- Mischke, S., Almogi-Labin, A., Ortal, R., Rosenfeld, A., Schwab, M.J., Boomer, I., 2010. Quantitative reconstruction of lake conductivity in the Quaternary of the Near East (Israel) using ostracods. *J. Paleolimnol.* 43, 667–688. <https://doi.org/10.1007/s10933-009-9359-y>.
- Mischke, S., Herzschuh, U., Massmann, G., Zhang, C., 2007. An ostracod-conductivity transfer function for Tibetan lakes. *J. Paleolimnol.* 38, 509–524. <https://doi.org/10.1007/s10933-006-9087-5>.
- Mischke, S., Zhang, C., 2010. Holocene cold events on the Tibetan Plateau. *Glob. Planet. Change* 72, 155–163. <https://doi.org/10.1016/j.gloplacha.2010.02.001>.
- National Meteorological Information Center, 2019. Monthly Standard Weather Station Dataset in Sanjiangyuan (1957–2015). <https://doi.org/10.11888/Meteoro.tpdc.270540>.
- Ning, D., Jiang, Q., Ji, M., Zheng, J., Kuai, X., Ge, Y., Xu, Y., Cheng, L., Zhao, W., 2022. Sedimentary black carbon isotope record of Holocene climate changes on the northeastern Tibetan Plateau. *Paleoceanog. Paleoclimatol.* 37, e2022PA004487. <https://doi.org/10.1029/2022PA004487>.
- Nichols, S.A., Shaw, B.H., 1986. Ecological life histories of the three aquatic nuisance plants, *Myriophyllum spicatum*, *Potamogeton crispus* and *Elodea canadensis*. *Hydrobiologia* 131, 3–21. <https://doi.org/10.1007/BF00008319>.
- Ohlendorf, C., Wennrich, V., Enters, D., 2015. Experiences with XRF-scanning of long sediment records. In: Croudace, I.W., Rothwell, R.G. (Eds.), *Micro-XRF Studies of Sediment Cores: Applications of a Non-destructive Tool for the Environmental Sciences*. Springer, Netherlands, Dordrecht, pp. 351–372. https://doi.org/10.1007/978-94-017-9849-5_13.
- Overpeck, J.T., Webb, T., Prentice, I.C., 1985. Quantitative interpretation of fossil pollen spectra: dissimilarity coefficients and the method of modern analogs. *Quat. Res.* 23 (1), 87–108. [https://doi.org/10.1016/0033-5894\(85\)90074-2](https://doi.org/10.1016/0033-5894(85)90074-2).
- Pang, H., Zhang, W., Wu, S., Jenk, T.M., Schwikowski, M., Hou, S., 2024. Abrupt climate fluctuations in Tibet as imprints of multiple meltwater events during the early to mid-Holocene. *Sci. Bull.* 69, 375–381. <https://doi.org/10.1016/j.scib.2023.12.007>.
- Parducci, L., Bennett, K.D., Ficetola, G.F., Alsos, I.G., Suyama, Y., Wood, J.R., Pedersen, M.W., 2017. Ancient plant DNA in lake sediments. *New Phytol.* 214, 924–942. <https://doi.org/10.1111/nph.14470>.
- Philbrick, C.T., 1983. Aspects of floral biology in three species of *Potamogeton* (pondweeds). *Mich. Bot.* 23, 35–38.
- Qiang, M., Jin, Y., Liu, X., Song, L., Li, H., Li, F., Chen, F., 2016. Late Pleistocene and Holocene aeolian sedimentation in Gonghe basin, northeastern Qinghai-Tibetan plateau: variability, processes, and climatic implications. *Quat. Sci. Rev.* 132, 57–73. <https://doi.org/10.1016/j.quascirev.2015.11.010>.
- R Core Team, 2021. *R: A Language and Environment for Statistical Computing*.
- Rørslett, B., 1991. Principal determinants of aquatic macrophyte richness in northern European lakes. *Aquat. Bot.* 39, 173–193. [https://doi.org/10.1016/0304-3770\(91\)90031-Y](https://doi.org/10.1016/0304-3770(91)90031-Y).
- Sayer, C., Roberts, N., Sadler, J., David, C., Wade, P.M., 1999. Biodiversity changes in a shallow lake ecosystem: a multi-proxy palaeolimnological analysis. *J. Biogeogr.* 26, 97–114. <https://doi.org/10.1111/j.1365-2699.1999.00298.x>.
- Schlütz, F., Lehmkuhl, F., 2009. Holocene climatic change and the nomadic Anthropocene in Eastern Tibet: palynological and geomorphological results from the Nianbaoyeze Mountains. *Quat. Sci. Rev.* 28, 1449–1471. <https://doi.org/10.1016/j.quascirev.2009.01.009>.
- Shang, Y., Wang, F., Sun, S., Zhu, B., Wang, P., 2023. Sources and transformations of nitrate in Qixiangcuo Lake and its inflow rivers in the northern Tibetan Plateau. *Environ. Sci. Pollut. Res.* 30, 4245–4257. <https://doi.org/10.1007/s11356-022-22542-7>.
- Solomina, O.N., Bradley, R.S., Hodgson, D.A., Ivy-Ochs, S., Jomelli, V., Mackintosh, A.N., Nesje, A., Owen, L.A., Wanner, H., Wiles, G.C., Young, N.E., 2015. Holocene glacier fluctuations. *Quat. Sci. Rev.* 111, 9–34. <https://doi.org/10.1016/j.quascirev.2014.11.018>.
- Søndergaard, M., Johansson, L.S., Lauridsen, T.L., Jørgensen, T.B., Liboriussen, L., Jeppesen, E., 2010. Submerged macrophytes as indicators of the ecological quality of lakes. *Freshw. Biol.* 55, 893–908. <https://doi.org/10.1111/j.1365-2427.2009.02331.x>.
- Song, C., Huang, B., Richards, K., Ke, L., Hien Phan, V., 2014. Accelerated lake expansion on the Tibetan Plateau in the 2000s: induced by glacial melting or other processes? *Water Resour. Res.* 50, 3170–3186. <https://doi.org/10.1002/2013WR014724>.
- Spence, D.H.N., 1967. Factors controlling the distribution of freshwater macrophytes with particular reference to the lochs of Scotland. *J. Ecol.* 55, 147–170. <https://doi.org/10.2307/2257723>.
- Stockmarr, J., 1971. Tables with spores used in absolute pollen analysis. *Pollen Spores* 13, 615–621.
- Stoof-Leichsenring, K.R., Huang, S., Liu, S., Jia, W., Li, K., Liu, X., Pestryakova, L.A., Herzschuh, U., 2022. Sedimentary DNA identifies modern and past macrophyte diversity and its environmental drivers in high-latitude and high-elevation lakes in Siberia and China. *Limnol. Oceanogr.* 67, 1126–1141. <https://doi.org/10.1002/lno.12061>.
- Stoof-Leichsenring, K.R., Liu, S., Jia, W., Li, K., Pestryakova, L.A., Mischke, S., Cao, X., Liu, X., Ni, J., Neuhaus, S., Herzschuh, U., 2020. Plant diversity in sedimentary DNA obtained from high-latitude (Siberia) and high-elevation lakes (China). *Biodivers. Data J.* 8, e57089. <https://doi.org/10.3897/BDJ.8.e57089>.
- Taberlet, P., Coissac, E., Pompanon, F., Gielly, L., Miquel, C., Valentini, A., Vermet, T., Corthier, G., Brochmann, C., Willerslev, E., 2007. Power and limitations of the chloroplast trn L (UAA) intron for plant DNA barcoding. *Nucleic Acids Res.* 35, e14. <https://doi.org/10.1093/nar/gkl938>.
- Tang, L., Mao, L., Shu, J., Li, C., Shen, C., Zhou, Z., 2020. *Atlas of Quaternary Pollen and Spores in China*. Springer Nature.
- ter Braak, C.J.F., Juggins, S., 1993. Weighted averaging partial least squares regression (WA-PLS): an improved method for reconstructing environmental variables from species assemblages. In: van Dam, H. (Ed.), *Twelfth International Diatom Symposium, Developments in Hydrobiology*. Springer, Netherlands, Dordrecht, pp. 485–502. https://doi.org/10.1007/978-94-017-3622-0_49.
- Väiranta, M., Kultti, S., Nyman, M., Sarmaja-Korjonen, K., 2005. Holocene development of aquatic vegetation in shallow Lake Njargajavri, Finnish Lapland, with evidence of water-level fluctuations and drying. *J. Paleolimnol.* 34, 203–215. <https://doi.org/10.1007/s10933-005-1840-7>.
- Väiranta, M., Salonen, J.S., Heikkilä, M., Amon, L., Helmens, K., Klimaschewski, A., Kuhry, P., Kultti, S., Poska, A., Shala, S., Veski, S., Birks, H.H., 2015. Plant macrofossil evidence for an early onset of the Holocene summer thermal maximum in northernmost Europe. *Nat. Commun.* 6, 6809. <https://doi.org/10.1038/ncomms7809>.
- Van Wijk, R.J., 1988. Ecological studies on *Potamogeton pectinatus* L. I. General characteristics, biomass production and life cycles under field conditions. *Aquat. Bot.* 31, 211–258. [https://doi.org/10.1016/0304-3770\(88\)90015-0](https://doi.org/10.1016/0304-3770(88)90015-0).
- Van Wijk, R.J., Van Goor, E.M.J., Verkley, J.A.C., 1988. Ecological studies on *Potamogeton pectinatus* L. II. Autecological characteristics, with emphasis on salt tolerance, intraspecific variation and isoenzyme patterns. *Aquat. Bot.* 32, 239–260. [https://doi.org/10.1016/0304-3770\(88\)90119-2](https://doi.org/10.1016/0304-3770(88)90119-2).
- von Hippel, B., Stoof-Leichsenring, K.R., Schulte, L., Seeber, P., Epp, L.S., Biskaborn, B. K., Diekmann, B., Melles, M., Pestryakova, L., Herzschuh, U., 2022. Long-term fungus-plant covariation from multi-site sedimentary ancient DNA metabarcoding. *Quat. Sci. Rev.* 295, 107758. <https://doi.org/10.1016/j.quascirev.2022.107758>.
- Wang, F., Qian, N., Zhang, Y., Yang, H., 1995. *Pollen Flora of China*, second ed. Science Press, Beijing.
- Wang, S., Dou, H., 1998. *Lakes in China*. Science Press, Beijing.
- Wang, W., Ji, M., 2007. Comparison on salt tolerance of nine submerged macrophytes. *J. Agro-Environ. Sci.* 26, 1259–1263.
- Weltje, G.J., 1997. End-member modeling of compositional data: numerical-statistical algorithms for solving the explicit mixing problem. *Math. Geol.* 29, 503–549. <https://doi.org/10.1007/BF02775085>.
- Weltje, G.J., Prins, M.A., 2007. Genetically meaningful decomposition of grain-size distributions. *Sediment. Geol.* 202, 409–424. <https://doi.org/10.1016/j.sedgeo.2007.03.007>.
- Weltje, G.J., Tjallingii, R., 2008. Calibration of XRF core scanners for quantitative geochemical logging of sediment cores: Theory and application. *Earth Planet Sci. Lett.* 274, 423–438. <https://doi.org/10.1016/j.epsl.2008.07.054>.
- Wischniewski, J., Herzschuh, U., Rühland, K.M., Bräuning, A., Mischke, S., Smol, J.P., Wang, L., 2014. Recent ecological responses to climate variability and human impacts in the Nianbaoyeze Mountains (eastern Tibetan Plateau) inferred from pollen, diatom and tree-ring data. *J. Paleolimnol.* 51, 287–302. <https://doi.org/10.1007/s10933-013-9747-1>.
- Woolway, R.I., Kraemer, B.M., Lenters, J.D., Merchant, C.J., O'Reilly, C.M., Sharma, S., 2020. Global lake responses to climate change. *Nat. Rev. Earth Environ.* 1, 388–403. <https://doi.org/10.1038/s43017-020-0067-5>.
- Wu, Z., Ding, Z., Yu, D., Xu, X., 2015. Influence of niche similarity on hybridization between *Myriophyllum sibiricum* and *M. spicatum*. *J. Evol. Biol.* 28, 1465–1475. <https://doi.org/10.1111/jeb.12667>.
- Yang, X., Kamenik, C., Schmidt, R., Wang, S., 2003. Diatom-based conductivity and water-level inference models from eastern Tibetan (Qinghai-Xizang) Plateau lakes. *J. Paleolimnol.* 30, 1–19. <https://doi.org/10.1023/A:1024703012475>.
- Yao, T., Bolch, T., Chen, D., Gao, J., Immerzeel, W., Piao, S., Su, F., Thompson, L., Wada, Y., Wang, L., Wang, T., Wu, G., Xu, B., Yang, W., Zhang, G., Zhao, P., 2022. The imbalance of the Asian water tower. *Nat. Rev. Earth Environ.* 3, 618–632. <https://doi.org/10.1038/s43017-022-00299-4>.
- Ye, Q., Yao, T., Zheng, H., Zhang, X., 2008. Glacier and lake co-variations and their responses to climate change in the Mapam Yumco Basin on Tibet. *Geogr. Res.* 27, 1178–1190. <https://doi.org/10.11821/jy2008050021>.
- Yu, S., Wang, J., Rühland, K.M., Zhu, L., Ju, J., Liu, C., Ma, Q., Smol, J.P., 2023. Spatial distribution of surface-sediment diatom assemblages from 45 Tibetan Plateau lakes and the development of a salinity transfer function. *Ecol. Indic.* 155, 110952. <https://doi.org/10.1016/j.ecolind.2023.110952>.
- Yu, S.-Y., Shen, J., Colman, S.M., 2007. Modeling the radiocarbon reservoir effect in lacustrine systems. *Radiocarbon* 49, 1241–1254. <https://doi.org/10.1017/S003822200043150>.
- Zhang, C., Mischke, S., 2009. A Lateglacial and Holocene lake record from the Nianbaoyeze Mountains and inferences of lake, glacier and climate evolution on the eastern Tibetan Plateau. *Quat. Sci. Rev.* 28, 1970–1983. <https://doi.org/10.1016/j.quascirev.2009.03.007>.
- Zhang, G., Yao, T., Xie, H., Yang, K., Zhu, L., Shum, C.K., Bolch, T., Yi, S., Allen, S., Jiang, L., Chen, W., Ke, C., 2020. Response of Tibetan Plateau lakes to climate

- change: trends, patterns, and mechanisms. *Earth Sci. Rev.* 208, 103269 <https://doi.org/10.1016/j.earscirev.2020.103269>.
- Zhang, Q., Dong, X., Yang, X., Liu, E., Lin, Q., Cheng, L., Liu, L., Jeppesen, E., 2022. Aquatic macrophyte fluctuations since the 1900s in the third largest Chinese freshwater lake (Lake Taihu): evidences, drivers and management implications. *Catena* 213, 106153. <https://doi.org/10.1016/j.catena.2022.106153>.
- Zhang, X., Xu, B., Xie, Y., Li, J., Li, Y., 2023. Continuous mass loss acceleration of Qiangyong Glacier, southern Tibetan plateau, since the mid-1880s inferred from glaciolacustrine sediments. *Quat. Sci. Rev.* 301, 107937 <https://doi.org/10.1016/j.quascirev.2022.107937>.
- Zhao, J., Liu, J., Liu, J., Chen, S., Wang, L., Zhou, A., Zhang, Z., Shen, Z., Chen, J., Chen, L., Cao, Y., 2023. Coupling of the ecosystems in North China with the East Asian summer monsoon rainfall during the Holocene. *Quat. Sci. Rev.* 300, 107885. <https://doi.org/10.1016/j.quascirev.2022.107885>.
- Zhao, Y., Yu, Z., Zhao, W., 2011. Holocene vegetation and climate histories in the eastern Tibetan Plateau: controls by insolation-driven temperature or monsoon-derived precipitation changes? *Quat. Sci. Rev.* 30, 1173–1184. <https://doi.org/10.1016/j.quascirev.2011.02.006>.
- Zhou, J., Wang, L., Zhang, Y., Guo, Y., Li, X., Liu, W., 2015. Exploring the water storage changes in the largest lake (Selin Co) over the Tibetan Plateau during 2003–2012 from a basin-wide hydrological modeling. *Water Resour. Res.* 51, 8060–8086. <https://doi.org/10.1002/2014WR015846>.
- Zhou, J., Wang, L., Zhong, X., Yao, T., Qi, J., Wang, Y., Xue, Y., 2022. Quantifying the major drivers for the expanding lakes in the interior Tibetan Plateau. *Sci. Bull.* 67, 474–478. <https://doi.org/10.1016/j.scib.2021.11.010>.
- Zhong, W., Pen, Z., Xue, J., Ouyang, J., Tang, X., Cao, J., 2012. Geochemistry of sediments from Barkol Lake in the westerly influenced northeast Xinjiang: implications for catchment weathering intensity during the Holocene. *J. Asian Earth Sci.* 50, 7–13. <https://doi.org/10.1016/j.jseas.2012.01.019>.